

High Energy Gamma-rays from Active Galactic Nuclei

Contents

1	Topics	5
1.1	ICRANet participants	5
1.2	Students	5
1.3	Ongoing collaborations	5
2	Brief description	7
3	Publications-2019	11
3.1	Publications-2012-2018	12
4	The Origin of the Multiwavelength Emission of PKS 0502+049	17
4.1	Introduction	17
4.2	Observations and Data Reduction	19
4.2.1	Fermi LAT	19
4.2.2	Swift XRT/UVOT observations	22
4.3	Spectral Analyses	23
4.4	Modeling of Broadband spectra	26
4.4.1	Hadronic γ -rays and neutrinos	26
4.4.2	Leptonic HE γ -rays	30
4.5	Discussion and Conclusions	33
5	Investigation of the Gamma-ray Spectrum of CTA 102 During the Exceptional Flaring State in 2016-2017	39
5.1	Introduction	39
5.2	Fermi LAT observations	42
5.3	Absorption of γ -rays	46
5.4	Origin of multiwavelength emission	49
5.4.1	Emitting region inside the BLR	50
5.4.2	Emitting region outside the BLR	51
5.5	Particle Acceleration and Energy losses	53
5.5.1	High energy cut-off in the electron spectrum	54

Contents

5.5.2	Power-law index of emitting electrons	56
5.6	Results and Discussion	57
5.7	Conclusions	59

1 Topics

- High energy gamma-rays from active galactic nuclei
- Galactic sources of high energy neutrinos
- High energy emission from gamma-ray bursts

1.1 ICRA Net participants

- Sahakyan Narek

1.2 Students

- Gasparyan Sargis
- Karlica Mile
- Harutyunyan Gevorg
- Israyelyan Davit
- Khachatryan Mher
- Mari Harutyunyan

1.3 Ongoing collaborations

- Razmik Mirzoyan (Max Planck Institute for Physics, Munich, Germany)
- Paolo Giommi (ASI Science Data Center)
- Damien Begue (Max Planck Institute for Extraterrestrial Physics, Munich, Germany)

1 Topics

- Ulisses Barres de Almeida (Centro Brasileiro de Pesquisas Físicas - CBPF/MCT)
- Bernardo Fraga (Centro Brasileiro de Pesquisas Físicas - CBPF)

2 Brief description

The main scientific activities of our group are in the field of X- and gamma-ray Astrophysics and Astroparticle physics. The results from the data analysis of Swift UVOT/XRT, NuStar, Chandra and Fermi LAT telescopes are used to investigate the particle acceleration and emission processes in the different classes of active galactic nuclei. The analysis of available data allows to investigate the emission processes and relativistic outflows in the most extreme regimes (keV-TeV).

Below we present several abstracts from the papers published in 2019.

- Origin of the multiwavelength emission of PKS 0502+049

The origin of the multiwavelength emission from PKS 0502+049 neighboring the first cosmic neutrino source TXS 0506+056 is studied using the data observed by Fermi-LAT and Swift UVOT/XRT. This source was in a flaring state in the considered bands before and after the neutrino observations in 2014-2015, characterized by hard emission spectra in the X-ray and γ -ray bands, $\simeq 1.5 - 1.8$ and ≤ 2.0 , respectively. During the neutrino observations, the γ -ray spectrum shows a deviation from a simple power-law shape, indicating a spectral cutoff at $E_c = 8.50 \pm 2.06$ GeV. The spectral energy distributions of PKS 0502+049 are modeled within a one-zone leptonic scenario assuming that high energy γ -ray emission is produced either by inverse Compton scattering of synchrotron or dusty torus photons by the electron population that produce the radio-to-optical emission. Alternatively, the observed γ -rays are modeled considering inelastic interaction of protons, when the jet interacts with a dense gaseous target. During the neutrino observations, the γ -ray data are best described when the proton energy distribution is $\sim E_p^{-2.61}$ and if the protons are effectively accelerated up to 10 PeV, the expected neutrino rate is ~ 1.1 events within 110 days. In principle, if the γ -ray emission with a hard photon index observed during the flaring periods extends up to \sim TeV, the expected rate can be somewhat higher, but such conditions are hardly possible. Within the hadronic interpretation, the γ -ray data can be reproduced only

when the accretion rate of PKS 0502+049 is in the supper-Eddington regime, as opposed to the leptonic scenario. From the point of view of the necessary energetics as well as considering that the required parameters are physically reasonable, when the neutrinos were observed, the broadband emission from PKS 0502+049 is most likely of a leptonic origin.

- Investigation of the Gamma-ray Spectrum of CTA 102 During the Exceptional Flaring State in 2016-2017

The flat spectrum radio quasar CTA 102 entered an extended period of activity from 2016 to 2017 during which several strong γ -ray flares were observed. Using Fermi large area telescope data a detailed investigation of γ -ray spectra of CTA 102 during the flaring period is performed. In several periods the γ -ray spectrum is not consistent with a simple power-law, having a hard photon index with an index of $\sim (1.8 - 2.0)$ that shows a spectral cutoff around an observed photon energy of $\sim (9 - 16)$ GeV. The internal γ -ray absorption via photon-photon pair production on the broad-line-region-reflected photons cannot account for the observed cut-off/break even if the emitting region is very close to the central source. This cut-off/break is likely due to a similar intrinsic break in the energy distribution of emitting particles. The origin of the spectral break is investigated through the multiwavelength modeling of the spectral energy distribution, considering a different location for the emitting region. The observed X-ray and γ -ray data is modeled as inverse Compton scattering of synchrotron and/or external photons on the electron population that produce the radio-to-optical emission which allowed to constrain the power-law index and cut-off energy in the electron energy distribution. The obtained results are discussed in the context of a diffusive acceleration of electrons in the CTA 102 jet.

- Open Universe for Blazars: a new generation of astronomical products based on 14 years of Swift-XRT data

Open Universe for blazars is a set of high-transparency multi-frequency data products for blazar science, and the tools designed to generate them. Blazars are drawing growing interest following the consolidation of their position as the most abundant type of source in the extragalactic very-high energy γ -ray sky, and because of their status as prime candidate sources in the nascent field of multi-messenger astrophysics. As such, blazar astrophysics is becoming increasingly data driven, depending on the integration and combined

analysis of large quantities of data from the entire span of observational astrophysics techniques. The project was therefore chosen as one of the pilot activities within the United Nations Open Universe Initiative. We aim to deliver innovative data science tools for multi-messenger astrophysics. In this work we developed a data analysis pipeline called Swift-DeepSky, based on the Swift XRTDAS software and the XIMAGE package, encapsulated into a Docker container. Swift-DeepSky, downloads and reads low-level data, generates higher-level products, detects X-ray sources and estimates several intensity and spectral parameters for each detection, thus facilitating the generation of complete and up-to-date science-ready catalogues from an entire space-mission dataset. The Docker version of the pipeline – whose concept can be reproduced with other missions – and its derived products is publicly available from the Open Universe Website at openuniverse.asi.it We present the results of a detailed X-ray image analysis based on Swift-DeepSky, that was run on all Swift XRT observations including a known blazar, carried out during the first 14 years of operations of the Neil Gehrels Swift Observatory. Short exposures executed within one week of each other have been added to increase sensitivity, which ranges between $\sim 1 \times 10^{-12}$ and $\sim 1 \times 10^{-14}$ erg cm⁻² s⁻¹ (0.3-10.0 keV). After cleaning for problematic fields, the resulting database includes over 27,000 images integrated in different X-ray bands, and a catalogue, called 1OUSXB, that provides intensity and spectral information for 33,396 X-ray sources, 8,896 of which are single or multiple detections of 2,308 distinct blazars. All the results can be accessed on-line in a variety of ways: e.g., from the Open Universe portal at openuniverse.asi.it, through Virtual Observatory services, via the VOU-Blazar tool and the SSDC SED builder. One of the most innovative aspects of this work is that the results can be safely reproduced and extended by anyone.

3 Publications-2019

- V. Acciari,.....S. Gasparyan...N. Sahakyan, D. Zaric, "Testing emission models on the extreme blazar 2WHSP J073326.7+515354 detected at very high energies with the MAGIC telescopes", *Monthly Notices of the Royal Astronomical Society*, Volume 490, Issue 2, p.2284-2299, 2019.
- R. Ruffini, R. Moradi, J. Rueda, L. Becerra, C. Bianco, C. Cherubini, S. Filippi, Y. Chen, M. Karlica, N. Sahakyan, Y. Wang, S. Xue, "On the GeV Emission of the Type I BdHN GRB 130427A", *The Astrophysical Journal*, Volume 886, Issue 2, article id. 82, 13 pp., 2019.
- V. Acciari,.....S. Gasparyan...N. Sahakyan, D. Zaric, "Observation of inverse Compton emission from a long γ -ray burst", *Nature*, Volume 575, Issue 7783, p.459-463, 2019.
- V. Acciari,.....S. Gasparyan...N. Sahakyan, D. Zaric, "Teraelectronvolt emission from the γ -ray burst GRB 190114C", *Nature*, Volume 575, Issue 7783, p.455-458, 2019.
- N. Sahakyan, "Origin of the multiwavelength emission of PKS 0502+049", accepted for publication in *Astronomy and Astrophysics*, doi.org/10.1051/0004-6361/201936715, arXiv:1911.12087, 2019.
- V. Acciari,.....S. Gasparyan...N. Sahakyan, D. Zaric, "New hard-TeV extreme blazars detected with the MAGIC telescopes", accepted for publication in *Astrophysical Journal Supplement*, arXiv:1911.06680, 2019.
- P. Giommi, C. Brandt, U. Barres de Almeida, A. Pollock, F. Arneodo, Y. Chang, O. Civitaresse, M. Angelis, V. DELia, J. Del Rio Vera, S. Di Pippo, R. Middei, A. Penacchioni, M. Perri, R. Ruffini, N. Sahakyan, S. Turriziani, "Open Universe for Blazars: a new generation of astronomical products based on 14 years of Swift-XRT data", *Astronomy and Astrophysics*, Volume 631, id.A116, 11 pp., 2019.

- T. Glauch, P. Padovani, P. Giommi, E. Resconi, B. Arsioli, N. Sahakyan, M. Huber, "Dissecting the region around IceCube-170922A: the blazar TXS 0506+056 as the first cosmic neutrino source", EPJ Web of Conferences, Volume 207, id.02003, 2019.
- V. Acciari,.....S. Gasparyan...N. Sahakyan, D. Zaric, "Constraints on Gamma-Ray and Neutrino Emission from NGC 1068 with the MAGIC Telescopes", The Astrophysical Journal, Volume 883, Issue 2, article id. 135, 9 pp., 2019.
- V. Acciari,.....S. Gasparyan...N. Sahakyan, D. Zaric, "Measurement of the extragalactic background light using MAGIC and Fermi-LAT gamma-ray observations of blazars up to $z = 1$ ", Monthly Notices of the Royal Astronomical Society, Volume 486, Issue 3, p.4233-4251, 2019.
- V. Acciari,.....S. Gasparyan...N. Sahakyan, D. Zaric, "Deep observations of the globular cluster M15 with the MAGIC telescopes", Monthly Notices of the Royal Astronomical Society, Volume 484, Issue 2, p.2876-2885, 2019.
- J. Rueda, R. Ruffini, Y. Wang, C. Bianco, J. Blanco-Iglesias, M. Karlica, P. Loren-Aguilar, R. Moradi, N. Sahakyan, "Electromagnetic emission of white dwarf binary mergers", Journal of Cosmology and Astroparticle Physics, Issue 03, article id. 044, 2019.
- N. Sahakyan, "Origin of the multiwavelength emission of PKS 0502+049", Astronomy and Astrophysics, Volume 622, id.A144, 10 pp. 2019.

3.1 Publications-2012-2018

- R. Ruffini, M. Karlica, N. Sahakyan, J. Rueda, Y. Wang, G. Mathews, C. Bianco, M. Muccino, "A GRB Afterglow Model Consistent with Hypernova Observations", The Astrophysical Journal, Volume 869, Issue 2, article id. 101, 9 pp. 2018.
- A. Abeysekara, ... N. Sahakyan, ... D. Zaric, "Periastron Observations of TeV Gamma-Ray Emission from a Binary System with a 50-year Period", The Astrophysical Journal Letters, Volume 867, Issue 1, article id. L19, 8 pp., 2018.

- P. Padovani, P. Giommi, E. Resconi, T. Glauch, B. Arsioli, N. Sahakyan, M. Huber, "Dissecting the region around IceCube-170922A: the blazar TXS 0506+056 as the first cosmic neutrino source", *Monthly Notices of the Royal Astronomical Society*, Volume 480, Issue 1, p.192-203, 2018.
- N. Sahakyan, "Lepto-hadronic γ -Ray and Neutrino Emission from the Jet of TXS 0506+056", *The Astrophysical Journal*, Volume 866, Issue 2, article id. 109, 6 pp. 2018.
- S. Gasparyan, N. Sahakyan, V. Baghmanyan, D. Zargaryan, "On the Multiwavelength Emission from CTA 102", *The Astrophysical Journal*, Volume 863, Issue 2, article id. 114, 11 pp., 2018.
- M. Aartsen, N. Sahakyan, T. Yuan, "Neutrino emission from the direction of the blazar TXS 0506+056 prior to the IceCube-170922A alert", *Science*, Volume 361, Issue 6398, pp. 147-151, 2018.
- V. Baghmanyan, M. Tumanyan, N. Sahakyan, Y. Vardanyan, "High-Energy γ -Ray Emission from PKS 0625-35", *Astrophysics*, Volume 61, Issue 2, pp.160-170, 2018.
- N. Sahakyan, V. Baghmanyan, D. Zargaryan, "Fermi-LAT observation of nonblazar AGNs", *Astronomy & Astrophysics*, Volume 614, id.A6, 11 pp., 2018.
- B. Fraga, U. Barres de Almeida, S. Gasparyan, P. Giommi, N. Sahakyan, "Time-Evolving SED of MKN421: a multi-band view and polarimetric signatures", *Frontiers in Astronomy and Space Sciences*, Volume 5, id.1, 2018.
- S. Gasparyan, N. Sahakyan, P. Chardonnet, "The origin of HE and VHE gamma-ray flares from FSRQs", *International Journal of Modern Physics D*, Volume 27, Issue 10, id. 1844007, 2018.
- D. Zargaryan, N. Sahakyan, H. Harutyunian, "Chandra observations of gamma-ray emitting radio galaxies", *International Journal of Modern Physics D*, Volume 27, Issue 10, id. 1844022, 2018.
- V. Baghmanyan, N. Sahakyan, "X-ray and γ -ray emissions from NLSy1 galaxies", *International Journal of Modern Physics D*, Volume 27, Issue 10, id. 1844001, 2018.

- D. Zargaryan, S. Gasparyan, V. Baghmanyanyan and N. Sahakyan, "Comparing 3C 120 jet emission at small and large scales", *Astronomy & Astrophysics*, Volume 608, id. A37, 10, 2017.
- U. Barres de Almeida, F. Bernardo, P. Giommi, N. Sahakyan, S. Gasparyann and C. Brandt, "Long-Term Multi-Band and Polarimetric View of Mkn 421: Motivations for an Integrated Open-Data Platform for Blazar Optical Polarimetry", *Galaxies*, vol. 5, issue 4, p. 90, 2017.
- V. Baghmanyanyan, S. Gasparyan and N. Sahakyan, "Rapid Gamma-Ray Variability of NGC 1275", *The Astrophysical Journal*, Volume 848, Issue 2, article id. 111, 8, 2017.
- N. Sahakyan and S. Gasparyan "High energy gamma-ray emission from PKS 1441+25", *Monthly Notices of the Royal Astronomical Society*, 470, 3, p.2861-2869, 2017.
- N. Sahakyan, V. Baghmanyanyan, and D. Zargaryan, "Gamma-ray Emission from Non-Blazar AGNs", *AIP Conference Proceedings*, Volume 1792, Issue 1, id.050002, 2017.
- N. Sahakyan and S. Gasparyan, "High Energy Gamma-Rays From PKS 1441+25", *AIP Conference Proceedings*, Volume 1792, Issue 1, id.050005, 2017.
- V. Baghmanyanyan, "Gamma-Ray Variability of NGC 1275", *AIP Conference Proceedings*, Volume 1792, Issue 1, id.050007, 2017.
- D. Zargaryan, "The Gamma-Ray Emission from Broad-Line Radio Galaxy 3C 120", *AIP Conference Proceedings*, Volume 1792, Issue 1, id.050008, 2017.
- N. Sahakyan, "Galactic sources of high energy neutrinos: Expectation from gamma-ray data", *EPJ Web of Conferences*, Volume 121, id.05005, 2016.
- Sahakyan, N., Zargaryan, D. and Baghmanyanyan, V. "On the gamma-ray emission from 3C 120", *Astronomy & Astrophysics*, Volume 574, id.A88, 5 pp., 2015.

- Sahakyan, N., Yang, R., Rieger, F., Aharonian, F. and de Ona-Wilhelmi, E. "High Energy Gamma Rays from Centaurus a" Proceedings of the MG13 Meeting on General Relativity ISBN 9789814623995, pp. 1028-1030, 2015.
- Sahakyan, N., Piano, G. and Tavani, M. "Hadronic Gamma-Ray and Neutrino Emission from Cygnus X-3", The Astrophysical Journal, Volume 780, Issue 1, article id. 29, 2014.
- Sahakyan, N., Rieger, F., Aharonian, F., Yang, R., and de Ona-Wilhelmi, E. "On the gamma-ray emission from the core and radio lobes of the radio galaxy Centaurus A", International Journal of Modern Physics: Conference Series, Volume 28, id. 1460182, 2014.
- Sahakyan, N., Yang, R. Aharonian, F. and Rieger, F., " Evidence for a Second Component in the High-energy Core Emission from Centaurus A?", The Astrophysical Journal Letters, Volume 770, Issue 1, L6, 2013.
- Yang, R.-Z., Sahakyan, N., de Ona Wilhelmi, E., Aharonian, F. and Rieger, F., "Deep observation of the giant radio lobes of Centaurus A with the Fermi Large Area Telescope", Astronomy & Astrophysics, 542, A19, 2012.
- Sahakyan, N., "High energy gamma-radiation from the core of radio galaxy Centaurus A", Astrophysics, 55, 14, 2012.
- Sahakyan, N., "On the Origin of High Energy Gamma-Rays from Giant Radio Lobes Centarus A", International Journal of Modern Physics Conference Series, 12, 224, 2012.

4 The Origin of the Multiwavelength Emission of PKS 0502+049

4.1 Introduction

The recent observations of Very High Energy (> 100 GeV; VHE) astrophysical neutrinos by IceCube [81, 1] has opened a new window on studying the nonthermal hadronic processes in the Universe. The neutrino events are distributed isotropically on the sky, suggesting they are of an extragalactic origin. Different source candidates and scenarios have been proposed to explain the origin of the observed neutrinos (e.g., see [93, 113, 150] and [13] for a review) but none of them has so far been statistically supported by the observational data.

The blazar sub class of active galactic nuclei is often considered as the most likely sources of VHE neutrinos. Such a consideration is natural considering the blazars are among the most luminous and energetic sources in the Universe. Blazars have two jets ejected in opposite directions, one of which is pointing towards the Earth and they are usually sub-grouped into flat spectrum radio quasars (FSRQs) and BL Lac objects, depending on the emission line properties [147]. The small inclination angle and the relativistic motion in the blazars jets substantially increase their apparent luminosity, so that their emission can be detected across the entire electromagnetic spectrum, from radio to High Energy (> 100 MeV; HE) or VHE γ -ray bands. The non-thermal Spectral Energy Distribution (SED) of blazars has two broad non-thermal peaks - one at the IR/optical/UV or X-ray and the other at HE γ -ray bands. The first peak is due to synchrotron emission of energetic electrons, while the second one can be explained by several different mechanisms. For example, in the so called Leptonic scenarios, the HE emission can be explained by inverse Compton scattering of synchrotron or external photons [68, 69, 138].

Generally, these leptonic scenarios are successfully applied to explain the observed properties in different bands, but sometimes fail to reproduce some observed features such as very fast variability almost in all observed bands (e.g., Mrk 501 [15] or PKS 2155-304 [11] etc.).

As an alternative, the HE emission can be explained by the interaction of energetic protons when they are effectively accelerated in the blazar jets. The HE component can be due to proton interaction either with a gaseous target (via proton-proton (pp) collisions; [50, 26, 28]) or with a photon field (proton- γ ($p\gamma$) when their energy exceeds the threshold of Δ resonance [103, 104, 102, 111, 112]) or due to proton synchrotron emission [111, 112]. The photomeson reaction ($p\gamma$) is more extensively used to explain the emission from blazars [37], as it is more likely to have a dense radiation target within the jet than a nuclear one (unless it is of an external origin).

Both types of blazars, FSRQs and BL Lacs, are usually considered as effective neutrino emitters. For example, [87] showed that one of the highest neutrino events detected so far (~ 2 PeV) possibly correlates with the bright flare of FSRQ PKS B1414-418. On the other hand, different models (e.g., [144, 143]) also predict neutrino emission from BL Lac objects: [120] showed spatial correlation between the extreme BL Lacs (emitting HE γ -rays above 50 GeV) and the arrival direction of the observed neutrino events, once more confirming the blazar-neutrino association.

Though blazar have been so far considered as the main sources of VHE neutrinos, no significant association between them and neutrino events has been found yet. The most promising candidate so far is the blazar TXS 0506+056 (with the coordinates of RA= 77.36 and Dec=+5.69) which can be associated with the neutrino event IceCube-170922A, detected on 22 September 2017 [83]. TXS 0506+056 is a bright blazar in the MeV/GeV band at the redshift of $z = 0.3365 \pm 0.001$ [122]. The multiwavelength observation campaign started after the neutrino alert showed that the source was in an active state almost in all electromagnetic bands, most interestingly, flaring in the HE and VHE γ -ray bands [83]. Moreover, IceCube has reported an independently observed 3.5σ excess of neutrinos from the direction of TXS 0506+056 between September 2014 and March 2015 [82], strengthening the association between the neutrino events and TXS 0506+056. Further, dissection in space, time, and energy of the region around the IceCube-170922A showed that in the γ -ray band the emission from the nearby flaring blazar PKS 0502+049 dominates at low energies, but TXS 0506+056 dominates the sky above energies of a few GeV [119]. Also, during the period of the neutrino excess in 2014-2015, the

γ -ray emission from TXS 0506+056 hardened with an excess of hard γ -ray radiation at the highest energies observable by Fermi Large Area Telescope (*Fermi*) [119]. All these make TXS 0506+056 the most probable source of the observed VHE neutrinos and many different scenarios have been already proposed to explain the observed neutrinos [17, 64, 46, 91, 114, 100, 149, 131]. In this paper, considering the interest toward the region of the sky with TXS 0506+056, the origin of the multiwavelength emission from the neighbouring bright source PKS 0502+049 (at $z = 0.954$ [56]) is investigated using the data from Swift UVOT/XRT and *Fermi* observations. This study is motivated by the fact that PKS 0502+049 is only $\sim 1.2^\circ$ far from TXS 0506+056 and in principle if the neutrinos are produced in the jet of PKS 0502+049 they can have some contribution into the IceCube observed events. The aims are: i) investigation of PKS 0502+049 emission properties when VHE neutrinos were observed, using the multiwavelength light curves, ii) testing of various emission scenarios modeling SEDs obtained in different periods and iii) estimation of the PKS 0502+049 neutrino emission rate assuming that the observed HE emission is due to interaction of protons. Such a study will be an independent test if, in the case when hadronic processes are responsible for the HE emission from PKS 0502+049, the produced neutrinos can have any contribution into the events observed by IceCube.

The paper is structured as follows. The *Fermi* and Swift UVOT/XRT data analyses are described in Sect. 4.2, while the spectral analyses are presented in Sect. 4.3. In Sect. 4.4 the modeling of broadband SEDs within leptonic and hadronic scenarios is presented. The results are discussed and summarized in Sect. 4.5.

4.2 Observations and Data Reduction

4.2.1 Fermi LAT

For the current study the *Fermi* [21] data accumulated during more than 9 years, from 4th August 2008 to 1st January 2018, are used. The 100 MeV - 300 GeV events from a $16.9^\circ \times 16.9^\circ$ square region of interest (ROI) around the γ -ray position of PKS 0502+049 (RA,dec)= (76.343, 4.998) were downloaded and analyzed using Fermi Science Tools v10r0p5 with P8R2_SOURCE_V6 instrument response function. The events are binned with *gtbin* tool into $0.1^\circ \times 0.1^\circ$ pixels and 34 logarithmically equal energy intervals. The standard cuts

4 The Origin of the Multiwavelength Emission of PKS 0502+049

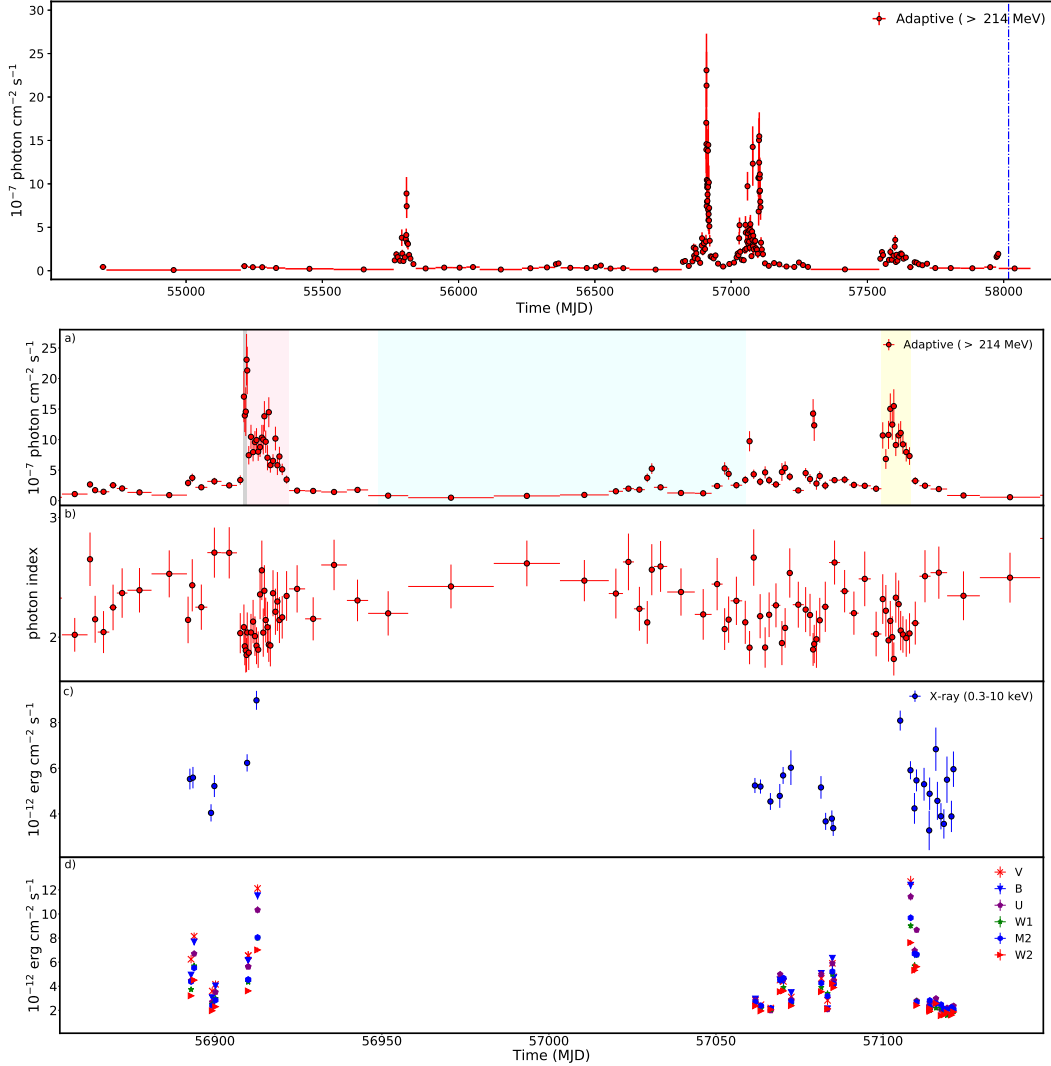


Figure 4.1 Top Panel: The γ -ray light curve of PKS 0502+049 above 214.0 MeV from August 4, 2008 to January 1st, 2018, with a constant uncertainty of 15%. Bottom Panels: (a) the γ -ray light curve and photon index (b), (c) X-ray and (d) optical/UV light curves are shown. The periods P1, P2 and P3 are marked with light gray, light red and light yellow colors, respectively, and the period when a 3.5σ excess of neutrinos between September 2014 and March 2015 was observed (P0) is in light blue. The blue dot-dashed line shows the period of detection of a HE neutrino event on September 22, 2017.

(e.g., on the maximum zenith angle (90°) to filter γ -rays from the Earth's limb) are applied with `gtselect` and `gtmktime` tools. The model file describing ROI was created using *Fermi* 8-year point source list ¹, including the sources within ROI+ 5° from the target and Galactic `gll_iem_v06` and isotropic `iso_P8R2_SOURCE_V6_v06` background models with the normalizations being free parameters. The normalization and spectral indices of the sources within ROI are left as free parameters while for the sources outside the ROI they are fixed to their values obtained during eight years of *Fermi* observations. Then, a binned maximum likelihood analyses is performed with the `gtlike` tool. Initially, the spectrum of PKS 0502+049 was modeled using a log-parabolic model [106] (as in the *Fermi* catalogs) but for the light curve calculations (for shorter periods) a power-law model was used.

The light curve generated by adaptive binning method has been used to investigate the flux variation in time. This novel method allows to identify not only different active states of the source but also find rapid changes in the γ -ray band. The considered period was divided into short (not equal) intervals assuming constant 15% uncertainty in each bin. The light curve calculated above $E_0 = 214$ MeV optimum energy (for calculation of E_0 see [101]) is shown in Fig. 4.1 (upper panel). The source quiescent state sometimes was followed by rapid and bright flaring periods. The most bright and prolonged γ -ray active period was observed from \sim MJD 56900 to MJD 57150, when the highest flux of $F_{>214\text{ MeV}} = (2.31 \pm 0.42) \times 10^{-6} \text{ photon cm}^{-2} \text{ s}^{-1}$ was observed on MJD 56909.5 for 4.81 hours. The photon index variation in time is presented in Fig. 4.1 b) which shows that the flux increase was accompanied by photon index hardening, the hardest one being 1.82 ± 0.14 significantly different than the photon index averaged over nine years (2.33 ± 0.02). This photon index is unusual for FSRQs which typically have a soft photon index in the MeV/GeV band but for several FSRQs occasionally such hard photon index was observed during rapid flares [133, 118, 66].

Then, the light curves during the flares are further analyzed. The flare rise and decay profiles could be constrained only for the bright period around MJD 57100 (see the light curve with one day bins in Fig. 4.2). The flare time profiles are analyzed using the double exponential form function given in [4] and the fit results are shown in Fig. 4.2 with blue line. The rise and decay times of the flare are $t_r = 2.00 \pm 0.35$ days and $t_d = 2.62 \pm 0.39$ days, respectively, with the flare peak at $t_p = t_0 + t_r t_d / (t_r + t_d) \ln(t_d / t_r) = \text{MJD } 57103.43$.

¹<https://fermi.gsfc.nasa.gov/ssc/data/access/lat/fl8y/>

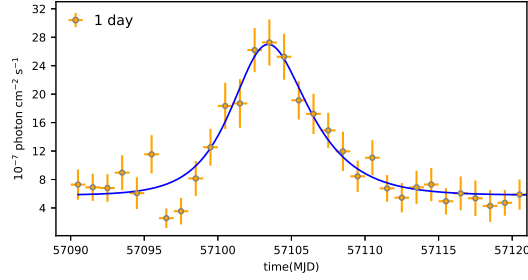


Figure 4.2 The light curve sub-interval with one-day bins for the flaring period. The blue line shows the flare fit with a double exponential function.

The constant level present in the flare is $(5.80 \pm 0.39) \times 10^{-7} \text{ photon cm}^{-2} \text{ s}^{-1}$ with the peak flux of $(4.20 \pm 0.23) \times 10^{-6} \text{ photon cm}^{-2} \text{ s}^{-1}$.

4.2.2 Swift XRT/UVOT observations

The Neil Gehrels Swift observatory (Swift) [67] observed PKS 0502+049 thirty-five times during the considered period. All the Swift observations were analyzed using the latest version of Swift data reduction software. The data were reprocessed with the standard filtering and screening criteria with the source- and background- extraction regions being defined correspondingly as a 20-pixel (47'') radius circular region and an annulus with inner and outer radii being 51 (120'') and 85 pixels (200''), respectively, both centered at the source position. For all observations, the count rate was below 0.5 count/s, implying no evidence of pile-up. Because of the small number of counts, the Cash statistic [42] on the unbinned data was used. The spectra were fitted with an absorbed power-law model in the 0.3-10 keV energy band with a neutral hydrogen column density fixed to its Galactic value $8.76 \times 10^{20} \text{ cm}^{-2}$ using XSPEC v12.9.1a [20].

The Swift XRT light curve is shown in Fig. 4.1 c) and the corresponding parameters are given in Table 4.1. Although the number of available observations is not sufficient for detailed temporal analyses, the X-ray flux increase during the bright γ -ray periods can be noticed. The highest X-ray flux of $(8.91 \pm 0.42) \times 10^{-12} \text{ erg cm}^{-2} \text{ s}^{-1}$ was observed on MJD 56912.78. No significant spectral evolution was observed in the X-ray band, the photon index most of the time being very hard $\sim (1.2 - 1.6)$ and the softest one being

$\Gamma_X \simeq 1.87 \pm 0.39$.

The Swift UVOT data have also been analyzed. The source counts were extracted from a circular region of a five-arcsec radius centred on the source, while the background counts from a surrounding annulus (source-free region) with the inner and outer radii being 27'' and 35'', respectively. Counts were converted to fluxes using `uvotsource` tool and zero-points from [38]. The magnitudes were corrected for extinction, using the reddening coefficient $E(B-V)$ from [136] and the ratios of the extinction to reddening $A_\lambda/E(B-A)$ for each filter from [61], then converting to fluxes following [38]. The averaged flux in Swift UVOT bands is given in Table 4.1 and shown in Fig. 4.1 d). During the γ -ray bright periods also the optical/UV flux has increased.

4.3 Spectral Analyses

The spectra obtained in the following periods are used for investigation of the origin of the multiwavelength emission from PKS 0502+049:

From MJD 56949.0 to 57059.0 (P0) corresponding to the neutrino observation window [82]. Swift observations around this period, Obsid: 33408003, 33408004, 33408005 and 33408006 were analyzed by merging them in order to increase the exposure and statistics as they have similar X-ray fluxes and photon indices.

From MJD 56908.60 to MJD 56909.80 (P1) during the largest γ -ray flaring period with available quasi-simultaneous Swift observation (Obsid: 33408001).

From MJD 56909.80 to MJD 56922.23 (P2) when the highest X-ray flux was observed (Obsid: 33408002) with a moderate brightening in the γ -ray band.

From MJD 57099.53 to MJD 57108.42 (P3), corresponding to another bright γ -ray flaring state coinciding with the Swift observation of Obsid: 33408009.

These periods are marked with light gray, light red, light blue and light yellow colors in Fig. 4.1 a). The γ -ray spectra were obtained applying an unbinned likelihood analyses method using a power-law model spectrum with the normalization and index considered as free parameters. After obtaining

Table 4.1 Summary of Swift XRT and UVOT observations of PKS 0502+049

Sequence No.	Log(Flux)	T	C-stat / dof	V	B	U	W1	M2	W2
00038377001	-12.08 ± 0.06	1.45 ± 0.16	0.77(89)	0.99 ± 0.11	0.83 ± 0.08	0.96 ± 0.06	0.97 ± 0.05	1.09 ± 0.06	0.87 ± 0.04
00038377002	-11.66 ± 0.05	1.45 ± 0.15	0.88(109)	---	---	1.43 ± 0.04	---	---	---
00038377003	-11.26 ± 0.03	1.44 ± 0.09	0.80(192)	6.24 ± 0.35	4.94 ± 0.23	4.47 ± 0.16	3.73 ± 0.14	4.38 ± 0.20	3.21 ± 0.12
00038377004	-11.25 ± 0.04	1.45 ± 0.10	0.95(196)	8.15 ± 0.30	7.68 ± 0.28	6.70 ± 0.25	5.69 ± 0.21	5.52 ± 0.20	4.51 ± 0.17
00038377005	-11.39 ± 0.04	1.54 ± 0.11	1.08(144)	3.59 ± 0.30	3.06 ± 0.20	2.69 ± 0.15	2.51 ± 0.14	2.39 ± 0.11	1.97 ± 0.11
00038377006	-11.28 ± 0.04	1.38 ± 0.11	0.93(181)	4.16 ± 0.31	4.03 ± 0.22	3.52 ± 0.16	2.99 ± 0.17	2.84 ± 0.10	2.30 ± 0.11
00033408001	-11.21 ± 0.03	1.53 ± 0.07	1.02(257)	6.54 ± 0.36	6.16 ± 0.23	5.63 ± 0.21	4.36 ± 0.16	4.55 ± 0.13	3.61 ± 0.13
00033408002	-11.05 ± 0.02	1.54 ± 0.06	1.33(343)	12.12 ± 0.33	11.52 ± 0.32	10.33 ± 0.29	8.00 ± 0.22	8.05 ± 0.22	7.01 ± 0.19
00033408003	-11.28 ± 0.03	1.46 ± 0.07	1.24(264)	2.83 ± 0.26	2.95 ± 0.22	2.82 ± 0.18	2.67 ± 0.15	2.69 ± 0.07	2.37 ± 0.11
00033408004	-11.28 ± 0.03	1.60 ± 0.07	0.97(262)	2.46 ± 0.16	2.12 ± 0.10	2.35 ± 0.09	2.14 ± 0.08	2.39 ± 0.11	1.95 ± 0.07
00033408005	-11.34 ± 0.03	1.48 ± 0.10	1.00(193)	2.18 ± 0.20	2.08 ± 0.17	1.99 ± 0.13	2.07 ± 0.11	2.18 ± 0.10	2.06 ± 0.09
00033408006	-11.32 ± 0.04	1.65 ± 0.13	0.87(114)	4.52 ± 0.42	4.54 ± 0.29	4.99 ± 0.18	4.52 ± 0.17	4.51 ± 0.29	3.55 ± 0.20
00033408007	-11.25 ± 0.03	1.65 ± 0.08	1.16(227)	4.40 ± 0.24	4.42 ± 0.16	4.59 ± 0.17	3.90 ± 0.14	4.68 ± 0.22	3.61 ± 0.13
00033408008	-11.22 ± 0.05	1.22 ± 0.14	1.02(115)	3.10 ± 0.29	3.48 ± 0.22	2.90 ± 0.19	2.48 ± 0.16	2.74 ± 0.18	2.39 ± 0.13
00033408009	-11.09 ± 0.02	1.85 ± 0.07	1.36(244)	30.72 ± 0.85	36.08 ± 0.66	33.9 ± 0.94	26.75 ± 0.49	24.76 ± 0.68	22.18 ± 0.41
00033408010	-11.23 ± 0.03	1.57 ± 0.08	1.05(216)	12.69 ± 0.47	12.40 ± 0.34	11.43 ± 0.32	9.02 ± 0.25	9.68 ± 0.27	7.62 ± 0.21
00033408011	-11.37 ± 0.06	1.57 ± 0.19	1.25(64)	---	---	6.95 ± 0.32	5.69 ± 0.31	6.70 ± 0.37	5.32 ± 0.25
00033408012	-11.26 ± 0.04	1.56 ± 0.11	1.54(151)	---	---	8.67 ± 0.24	6.60 ± 0.24	6.63 ± 0.24	5.62 ± 0.16
00033408013	-11.28 ± 0.06	1.52 ± 0.16	0.75(87)	---	---	2.79 ± 0.21	2.75 ± 0.20	2.67 ± 0.22	2.41 ± 0.13
00033408014	-11.48 ± 0.10	1.87 ± 0.39	1.10(26)	---	---	2.39 ± 0.18	2.07 ± 0.15	2.30 ± 0.19	2.00 ± 0.13
00033408015	-11.31 ± 0.06	1.60 ± 0.17	1.13(78)	---	---	2.55 ± 0.19	2.01 ± 0.17	2.24 ± 0.21	1.91 ± 0.12
00033408016	-11.17 ± 0.06	1.21 ± 0.14	0.96(97)	---	---	2.67 ± 0.20	2.27 ± 0.17	2.82 ± 0.23	2.16 ± 0.14
00033408017	-11.34 ± 0.07	1.60 ± 0.21	0.73(54)	---	---	2.98 ± 0.22	2.20 ± 0.22	2.57 ± 0.24	2.57 ± 0.21
00033408018	-11.41 ± 0.06	1.85 ± 0.20	1.19(60)	---	---	2.04 ± 0.17	2.18 ± 0.18	2.48 ± 0.21	1.56 ± 0.12
00033408019	-11.45 ± 0.07	1.51 ± 0.21	0.94(58)	---	---	2.04 ± 0.17	1.99 ± 0.17	2.12 ± 0.20	1.62 ± 0.12
00033408020	-11.26 ± 0.07	1.17 ± 0.20	1.31(69)	---	---	2.20 ± 0.18	1.58 ± 0.16	2.06 ± 0.19	1.81 ± 0.13
00033408021	-11.41 ± 0.07	1.41 ± 0.19	0.98(63)	---	---	2.28 ± 0.17	1.96 ± 0.16	2.24 ± 0.19	1.61 ± 0.10
00033408022	-11.22 ± 0.05	1.48 ± 0.15	1.21(98)	---	---	2.37 ± 0.20	1.90 ± 0.16	2.08 ± 0.19	1.86 ± 0.12
00033662001	-11.29 ± 0.04	1.40 ± 0.11	1.11(156)	4.65 ± 0.34	5.07 ± 0.23	4.99 ± 0.23	3.90 ± 0.18	4.26 ± 0.12	3.55 ± 0.16
00033662002	-11.43 ± 0.04	1.66 ± 0.13	1.10(126)	2.83 ± 0.42	2.13 ± 0.22	2.08 ± 0.15	3.40 ± 0.09	3.18 ± 0.26	2.12 ± 0.16
00033662003	-11.47 ± 0.04	1.69 ± 0.13	1.14(138)	4.78 ± 0.35	4.71 ± 0.26	4.43 ± 0.20	4.12 ± 0.19	4.19 ± 0.23	3.89 ± 0.11
00033662004	-11.42 ± 0.04	1.51 ± 0.11	1.33(145)	5.91 ± 0.38	6.33 ± 0.23	5.89 ± 0.22	5.00 ± 0.14	5.22 ± 0.48	4.23 ± 0.16

the best-fit values we fix them for the SED calculations.

The results are shown in Fig. 4.3 and the corresponding parameters in Table 4.2. The γ -ray spectrum contemporaneous with the IceCube observational window (~ 110 days; gray) follows the same tendency as that averaged over nine years (light gray) while the γ -ray spectra in the active periods (blue, red and magenta) are significantly different. There is an evident curvature in the γ -ray spectra obtained during P0 (see also [99]) so an alternative fit with power law with an exponential cut-off model in the form of $dN/dE \sim E_\gamma^{-\alpha} \times \text{Exp}(-E_\gamma/E_{cut})$ and a log-parabolic function in the form of $dN/dE \sim (E_\gamma/E_{br})^{-(\alpha+\beta \log(E_\gamma/E_{br}))}$ were applied to check if the curvature in the spectrum is statistically significant. The models are compared using a log likelihood ratio test: the significance is the square root of twice the difference in the log likelihoods. The first model with $\alpha = 2.07 \pm 0.04$ and $E_{cut} = 8.50 \pm 2.06$ GeV is preferred over the power-law model with a significance of 7.36σ . Also, the second model with $\alpha = 2.23 \pm 0.02$ and $\beta = 0.11 \pm 0.01$ is preferred with a significance of 6.82σ . The curvature in the blazar emission spectra can be due to different reasons. For example, log-parabolic spectra can be formed when the leptons in the jet undergo stochastic acceleration; power law with an exponential cut-off spectrum is expected when the energy distribution of the emitting electrons has a sharp energy upper cut-off because of the efficiency of the acceleration mechanisms. These results show that the γ -ray emission from PKS 0502+049 and consequently the spectra of particles responsible for the emission were characterized by a cut-off at tens of GeV when the neutrino events were detected by IceCube. Interestingly, during the flares before (P1 and P2) and after (P3) this period the γ -ray spectra extend up to tens of GeV with a significantly harder photon index, for example $\Gamma = 1.88 \pm 0.06$ during P1 and $\Gamma \simeq 2.0$ during P2 and P3, implying that VHE photons are dominating. This substantial hardening might be caused by injection of new (fresh) particles and/or a change in the location of the emission region where the acceleration is more efficient or the cooling is rather slow allowing the particles to reach higher energies. For generating X-ray spectra, again Cash statistic on Swift unbinned data was applied. Then, in order to increase the significance of individual points in the SEDs calculations, a denser rebinning was applied, restricting the energy range to > 0.5 keV. The results of the fit are given in Table 4.1 (similar parameters for the merged observations are: $\Gamma_X = 1.56 \pm 0.04$, $F_{X(0.3 - 10 \text{ keV})} = (4.85 \pm 0.15) \times 10^{-12} \text{ erg cm}^{-2}\text{s}^{-1}$) and the correspond-

Table 4.2 Parameters of γ -ray spectral analysis

Period	Flux	Photon Index	σ
9 years	1.19 ± 0.04	2.33 ± 0.02	105.3
MJD 56949.00-57059.00	4.17 ± 0.16	2.23 ± 0.02	65.9
MJD 56908.60-56909.80	32.88 ± 3.37	1.88 ± 0.06	28.9
MJD 56909.80-56922.23	17.42 ± 0.85	2.08 ± 0.03	56.8
MJD 57099.53-57108.42	20.82 ± 1.16	2.01 ± 0.04	48.0

ing spectra are shown in Fig. 4.3. During the bright γ -ray periods both the optical/UV and X-ray fluxes increased: the observed shape of UVOT data suggest that it corresponds to the HE tail of the synchrotron component while the hard X-ray spectra are due to the second emission component (in the case of leptonic interpretation).

4.4 Modeling of Broadband spectra

As it has been already noted, there are two conceptually different mechanisms which can be responsible for the HE component in blazar emission spectra. The theoretical models are generally divided into leptonic and hadronic ones depending on whether the electrons or protons are responsible for the emission. Here, the multiwavelength emission of PKS 0502+049 is discussed within both leptonic and hadronic emission scenarios.

4.4.1 Hadronic γ -rays and neutrinos

In the hadronic or lepto-hadronic blazar jets emission scenarios, the relativistic jet material is composed of protons (p) and electrons (e) that start to emit when accelerated to ultra-high energies. The low-energy component is dominated by direct synchrotron emission of electrons while the HE component is completely or partially formed due to the radiative output of energetic protons. The blazar jets are ideal laboratories where the protons are sometimes accelerated to above 10^{18} eV [104] and their energy is converted into electromagnetic power either due to interaction with gaseous [28, 24, 19, 27, 52] or photon targets [103, 104, 102, 111, 112] and/or via synchrotron emission [111, 112]. These channels might, in fact, operate simultaneously in a com-

peting way and contribute to the total energy loss of protons.

One of the scenarios most widely applied to explain the HE emission component assumes that the protons interact with the photon field of an internal (e.g., synchrotron photons) or external (e.g., disc photon reflected from Broad Line Region (BLR) or from dusty torus) origin. Then, γ -rays, neutrinos and electron-positron pairs (e^- , e^+) are produced from the decay of neutral and charged pions. The γ -rays and e^-, e^+ pairs will interact and initiate an electromagnetic cascade that will reduce the energy of the electromagnetic component down to energies at which the source becomes transparent to the $\gamma\gamma$ pair production. In this case, the spectra of the produced neutrinos can be well constrained when the data above 100 GeV are present which are missing for PKS 0502+049. Roughly, assuming that in the $p\gamma$ interactions comparable energy is released into the electromagnetic component (from X- to γ -rays) and neutrinos, $\phi_\gamma \simeq 4\phi_\nu$ (e.g., [74, 73]), some constraints on the expected neutrino flux can be imposed. For the X- to γ -ray emission spectrum in the form of $dN_\gamma/dE_\gamma = N_{0,\gamma}(E_\gamma/100\text{ eV})^{-\Gamma_\gamma} \text{Exp}(-E_\gamma/E_{cut})$ (the power-law spectrum gives poor modeling), the energy flux carried by the electromagnetic component is $\phi_\gamma \simeq 9.81 \times 10^{-11} \text{ erg cm}^{-2} \text{ s}^{-1}$ estimated by fitting the observed data. In this case, the differential spectrum of the accompanying neutrinos can be estimated from $dN_\nu/dE_\nu = (2 - \Gamma_\nu)/(E_{\nu,2}^{2-\Gamma_\nu} - E_{\nu,1}^{2-\Gamma_\nu})\phi_\gamma E_\nu^{-\Gamma_\nu}$ which predicts a flux of $\simeq 6.55 \times 10^{-16} \text{ TeV}^{-1} \text{ cm}^{-2} \text{ s}^{-1}$ at 100 TeV assuming a spectral index of 2.1 ± 0.2 , adopting $E_{\nu,min} = 1 \text{ TeV}$ and $E_{\nu,max} = 10 \text{ PeV}$. Even if this is a very strict upper limit (the exact estimations require simulations of the proton acceleration and emission processes as well as detailed tracking of cascade propagation) it is already lower than the IceCube measured flux.

The next scenario for neutrino emission from blazar jets assumes that a dense and compact target (e.g., cloud(s) from BLR [50, 26, 18] or a star/star envelope [28, 24, 19, 27, 52]) crosses the jet and the accelerated protons penetrating into it interact with the target protons. Depending on the number of jet-crossing targets, the emission can appear as steady (e.g., several clouds can interact with the jet simultaneously) or flare-like. Proton-proton (pp) interactions produce neutral (π^0) and charged pions (π^\pm) which then decay into γ -rays ($\pi^0 \rightarrow \gamma\gamma$) and neutrinos ($\pi^+ \rightarrow \mu^+ + \nu_\mu \rightarrow e^+ + \nu_e + \nu_\mu + \bar{\nu}_\mu$). Unlike the case of $p\gamma$ interaction scenario, a radiation in the MeV/GeV bands is also produced, so the γ -ray data can be used to constrain the proton content in the jet. One of the key points in the jet-target interaction scenario is the acceleration of protons to energies necessary for production of the observed

γ -rays and neutrinos; depending on the distance from the base of the jet, where the penetration occurs, the protons can be either accelerated in the jet or in the target when a strong shock is formed, and their energy can go well beyond 10 PeV (a simple relation between the proton acceleration region size R and cooling time scale yields $E_{max} \simeq 3.0 \times 10^{15} (\eta/0.1) (B/1G) (R/10^{13}cm)$ eV [131]).

The jet-target interaction scenario requires several parameters for accurate estimation of the duration, rate and efficiency of interactions. Especially, the parameters describing the target are needed for calculating the related radiative outputs and estimation of the required total energy of protons. In this case, we do not specify the origin of the dense target and only consider its density indirectly constrained by the observations. Namely, the estimated variability of $t_v \simeq 2$ days can be used to define the density of the target (n_H), i.e., comparing it with the characteristic cooling time of pp interactions, $t_{pp} \simeq (K\sigma_{pp}n_H)^{-1} \simeq 10^{15}/n_H$, so $n_H = 5.78 \times 10^9 cm^{-3}$ which is not significantly different from the usually estimated values. As this target density is high, the protons lose a significant fraction of their energy at pp collisions: the interaction is in a radiatively efficient regime, $t_{pp} \leq t_v$, so most of the γ -rays are emitted around t_v rather than when the target is already accelerated to high velocities.

The γ -ray spectra of PKS 0502+049 observed in different periods are modeled by expressing the energy distribution of energetic protons as $N_p(E_p) \sim E_p^{-\alpha_p} \exp(-E_p/E_{p,c})$, where the cut-off energy $E_{p,c}$ is initially considered as a free parameter and then fixed to an arbitrary value of $E_{c,p} = 10$ PeV; this is selected to ensure the produced neutrinos will have energy above 100 TeV, but, in principle, a cutoff at much higher energies cannot be excluded. In order to constrain the model parameters more efficiently (the normalization of proton content and their power-law spectral index), i.e., to find the parameters which statistically better explain the observed data, the Markov Chain Monte Carlo (MCMC) method is employed. This allows to derive the best-fit and uncertainty distributions of the spectral model parameters through MCMC sampling of their likelihood distributions [151]. The neutrino spectra above 100 GeV are calculated following [92] while at lower energies a delta function approximation is used (for exact formula see [134]).

In the inset of Fig. 4.3, the data observed during P0, P1 and P2 are modeled as γ -rays from the decay of neutral pions (π^0). During the neutrino observation in 2014-2015, when the power-law index and cut-off in the pro-

ton spectrum are considered as free parameters, the data are best described when $\alpha_p = 2.60 \pm 0.06$ and $E_{p,c} = 3.36 \pm 2.95$ TeV. The power-law index is mostly defined by the observed γ -ray photon index, whereas the cut-off with a large statistical uncertainty is constrained by the last point in the γ -ray spectrum. When the cutoff is fixed to much larger values, $E_{p,c} = 10$ PeV (solid gray line), the data can be reproduced when $\alpha_p = 2.61 \pm 0.06$ which predicts also an emission beyond the observed γ -ray data. Due to the steep spectrum of emitting protons, the γ -ray emission is dominated by the decay of π^0 with a negligible contribution from secondary particles produced by the decay of charged pions. On the other hand, such a steep spectrum also disfavors the possibility of producing a detectable flux of VHE neutrinos. The hardest power-law index when the observed data can be still explained is $\alpha_{p,c} = 2.2$ (gray dot-dashed line); however, this will heavily overpredict the γ -ray data above ~ 2 GeV. Within the applied scenario, the γ -ray spectra observed during the bright P1 and P2 periods can be also modeled (blue and solid lines) when harder indices of $\alpha_p = 2.14 \pm 0.10$ and $\alpha_p = 2.23 \pm 0.07$ are considered, respectively. Again, the cut-off energy cannot be constrained by the data and, in principle, strong emission of γ -rays and neutrinos up to VHEs can be expected.

In this interpretation the total energy of protons (above 1 GeV) in the jet as well as their luminosity can be estimated. Defining the luminosity as $L_{pp} = W_{pp}/t_{pp}$ where $W_{pp} = \int E_p N_p(E_p) dE_p$ is the total proton energy integrated from $E_{p,min}$ to $E_{p,max}$ and $t_{pp} = 2$ days is the cooling time of protons, the γ -ray data averaged over the IceCube observational window can be modeled when $L_{pp} \simeq 1.60 \times 10^{49} \text{ erg s}^{-1}$. This luminosity can be as large as $L_{pp} \simeq 2.60 \times 10^{50} \text{ erg s}^{-1}$ when the γ -ray active periods are considered. These estimations show that if the γ -rays from PKS 0502+049 are indeed produced in pp interactions then its jet should be very powerful and efficient in order to transfer a large amount of energy to protons.

Constraining the energy distribution of protons and their luminosity, the differential spectrum of the accompanying neutrinos can be calculated straightforwardly. Then, the number of neutrinos detected in a certain exposure of t_{exp} can be estimated from $N_\nu \simeq t_{exp} \int A_{eff}(E_\nu) dN_\nu/dE_\nu dE_\nu$, using the effective area $A_{eff}(E_\nu)$ from [2]. The neutrino rate (> 200 GeV) expected within ~ 110 days can be as large as ~ 1.1 events when the energy distribution of protons follows $E_p^{-2.61}$ with a cutoff at 10 PeV. In principle a higher rate (> 20) is possible when $\alpha_{p,c} = 2.2$ is considered but in this case the γ -ray data above

1 – 2 GeV cannot be explained. This is similar to the case applied in [80] where again the γ -ray emission from PKS 0502+049 was interpreted within a jet-target interaction scenario but using a harder proton index. As in this case, the γ -ray data are not well explained when $\alpha_p \leq 2.0$ which is natural considering the observed steep spectrum in the γ -ray band; when pp interaction is considered, the produced γ -rays will have nearly the same spectra as those of parent protons, $\alpha_\gamma \simeq \alpha_p - 0.1$. In principle, a hard power-law index of the protons is possible when normalizing it with the sub-GeV γ -ray data, but then a sharp cutoff will be required to describe the observed break at $E_{c,\gamma} = 8.50 \pm 2.06$ GeV. Even at the most unrealistic case when $E_{c,p} = 10^4 \times E_{c,\gamma}$, the neutrino spectrum, $\sim E_\nu^{-\alpha_\nu} \exp(-\sqrt{E_\nu/E_{\nu,c}})$ where $E_{\nu,c} \simeq E_{c,p}/40$ [88], will drop above ~ 2.1 TeV predicting almost no VHE neutrinos. Also, the expected number of neutrinos is somewhat uncertain when the γ -ray active periods are considered, as it strongly depends on the energy cut-off which is unknown. For example, when the cut-off at 10 PeV is considered, the neutrino rate is 14.7 and 22.1 during P1 and P2, respectively, while in the case of ~ 10 TeV it is as low as ~ 0.75 . This makes any possible claim for neutrino detection during the active periods significantly uncertain.

4.4.2 Leptonic HE γ -rays

In the view of the problems in the hadronic scenarios applied (e.g., the required energetics), the observed broadband emission from PKS 0502+049 is discussed also within a leptonic scenario. The multiwavelength spectra for different periods are shown in Fig. 4.3 where the archival radio-optical data from ASI science data center and the γ -ray spectra averaged over nine years are shown in light-gray. The spectra in the period when VHE neutrinos were observed (P0) is shown in gray. During the γ -ray active periods the flux increases in all other bands as well, and both components are shifted to higher energies. Here, in the leptonic interpretations, the broadband emission from PKS 0502+049 is modeled within the one-zone synchrotron/synchrotron self Compton [105, 35, 68] plus external inverse Compton [139, 69, 33] scenarios. In the framework of one-zone leptonic scenarios, the low energy emission (radio through optical) is described by the synchrotron emission of leptons in the magnetic field (B), while the HE component (from X-ray to HE γ -ray) is due to the inverse Compton scattering of internal photons, e.g., synchrotron photons (synchrotron self-Compton [SSC]) or external photons (EIC), e.g., emit-

ted from the IR dusty torus. Within this scenario, it is assumed a spherical region (blob) with a comoving radius R_b is moving with a bulk Lorentz factor Γ_b toward the observer and is filled with an isotropic population of electrons and a randomly oriented uniform magnetic field B . The energy spectrum of the injected electrons in the jet frame can be expressed as (e.g., [84])

$$N'_e(E'_e) = N'_0 \left(E'_e / m_e c^2 \right)^{-\alpha} \text{Exp}[-E'_e / E'_{cut}] \quad (4.4.1)$$

for $E'_{min} \leq E'_e \leq E'_{max}$ where E'_{min} and E'_{max} are the minimum and maximum electron energies, respectively. The emitted radiation will be Doppler-boosted by δ which equals to the bulk Lorentz factor for the small jet viewing angles. For the Doppler factor, a typical value of 20 [71] will be adopted which is usually used for the modeling of emission from FSRQs. The radius of the emission region can be constrained by the variability time scales: the radius can not be larger than $R_b \leq c \times t \times \delta / (1 + z) \simeq 5.31 \times 10^{16} (\delta/20) \text{ cm}$. Usually, the Compton dominance (domination of the second emission peak) observed from FSRQs can be explained by inverse Compton scattering of the external photon fields. If the jet dissipation occurs within the BLR with a radius of $7.6 \times 10^{17} \text{ cm}$ for PKS 0502+049 (measured using $R_{BLR} \sim \lambda L_\lambda (5100 \text{ \AA})^{0.7}$ relation [117]) the dominant external photon fields are disc photons reflected by the BLR clouds. On the other hand, the recent observations in the VHE γ -ray band indicate that the emission region can be also well beyond the BLR where the dominant photon field is IR radiation of the dust torus [7, 14, 16]. These regions appear more favorable for the VHE γ -ray emission (e.g., [66]). In the current study the torus photons are taken into account assuming the emission from the torus has a blackbody spectrum with a temperature of $T = 10^3 \text{ K}$ and fills a volume that for simplicity is approximated as a spherical shell with a radius of $R_{IR} = 3.54 \times 10^{18} (L_{disc} / 10^{45})^{0.5} \text{ cm}$ [116]. The corresponding radiation energy density, as measured in the comoving frame would be $u_{torus} = \eta L_{disc} \delta^2 / 4\pi R_{torus}^2 c \simeq 5.1 \times 10^{-2} (\delta/20)^2 \text{ erg cm}^{-3}$ where $\eta = 0.6$ [70]. During the fitting, the model free parameters (magnetic field and parameters describing the nonthermal electron distribution) and their uncertainties are estimated applying the MCMC method using *naima* package [151].

The modeling of SEDs observed during, P0, P1 and P2 are shown in Fig. 4.3 and the corresponding parameters are given in Table 4.3. In all modeling, the radio data are not considered as they are not simultaneous and

Table 4.3 Parameters of γ -ray spectral analysis

	P0	P1	P2
α	1.82 ± 0.02	1.61 ± 0.05	1.90 ± 0.07
E'_{min} [MeV]	12.97 ± 7.17	14.71 ± 8.59	65.68 ± 23.70
E'_c [GeV]	7.76 ± 0.39	2.51 ± 0.20	1.99 ± 0.14
E'_{max} [TeV]	0.63 ± 0.29	0.58 ± 0.35	0.68 ± 0.28
B [mG]	31.27 ± 0.61	102.92 ± 8.03	235.93 ± 8.17
L'_B [$erg\ s^{-1}$]	4.13×10^{42}	4.48×10^{43}	2.35×10^{44}
L'_e [$erg\ s^{-1}$]	1.87×10^{46}	7.52×10^{45}	4.26×10^{45}

the emission in this band can be produced from the low-energy electrons in more extended regions. Initially, the HE component observed during P0 is modeled considering only SSC mechanisms (gray dot-dashed line) as due to compactness of the emitting region the density of synchrotron photons might be dominating. The observed data are relatively well explained when $E'_{min} = 12.97 \pm 7.17$ MeV, $\alpha = 1.82 \pm 0.02$ and $E'_c = 7.76 \pm 0.39$ GeV. However, as the HE component exceeds that at lower energies, this modeling requires a strongly particle-dominated jet $U_e/U_B \simeq 4.5 \times 10^3$ for $B = 31.27 \pm 0.61$ mG. The required extreme parameters can be softened when the contribution from external photons is considered. For example, the solid gray line represents the modeling of the data considering inverse Compton scattering of both synchrotron and torus photons. This requires a softer power-law index for the electrons $\alpha = 2.42 \pm 0.28$ and as the energy of torus photons exceeds the averaged energy of synchrotron ones, this modeling requires lower minimum and cutoff energies of $E'_{min} = 5.91 \pm 0.61$ MeV and $E'_c = 2.91 \pm 0.21$ GeV, respectively. In this case, the synchrotron emission of the low energy electrons will exceed the observed radio flux a few times but as the radio data are not contemporaneous, this cannot be a strong argument to disfavor such modeling. Unlike the previous case, the system is close to equipartition $U_e/U_B \simeq 19.6$. Similarly, the spectra observed in bright P1 and P2 are modeled considering the SSC and EIC mechanisms. For both periods, the optical/UV and X-ray data can be explained by synchrotron/SSC emission while the γ -ray data are due to the inverse Compton scattering of external photons from dusty torus. During P1 the power-law index of emitting electrons was $\alpha = 1.61 \pm 0.05$ defined by the hard γ -ray photon index, while it was $\alpha = 1.90 \pm 0.07$ during P2 when a nearly flat spectrum in the γ -ray

band was observed. The cut-off energy of $E'_{cut} = 1.99 - 2.51$ GeV is measured from the optical/UV data which is not significantly different for the two periods. The magnetic field in P2 ($B = 235.93 \pm 8.17$ mG) is slightly larger than that in P1 ($B = 102.92 \pm 8.03$ mG) in agreement with the observed increase in the optical/UV bands. The total luminosity of the jet defined as $L_{jet} = L_B + L_e$ where $L_B = \pi c R_b^2 \Gamma^2 U_B$ and $L_e = \pi c R_b^2 \Gamma^2 U_e$ [43] is in the range of $L_{jet} \simeq (4.50 - 7.56) \times 10^{45} \text{ erg s}^{-1}$. During P1 the jet is particle-dominated with $U_e/U_B = 167.9$ while for P2 $U_e/U_B = 18.1$.

4.5 Discussion and Conclusions

Blazar jets have always been assumed as the most promising sources of VHE neutrino emission. The recent association between the IceCube-170922A neutrino event with the γ -ray bright BL Lac object TXS 0506+056 has opened new perspectives for investigation of the blazar jets physics. For the first time, the emission processes in relativistic jets can be studied using both γ -rays and neutrinos. Though there are various arguments favoring TXS 0506+056 as the main source for the observed VHE neutrinos, additional care must be taken when considering the presence of the nearby powerful γ -ray emitter- PKS 0502+049. In this paper the origin of the multiwavelength emission from FSRQ PKS 0502+049 is investigated aiming to verify whether or not the possible neutrino emission from PKS 0502+049 accompanying the observed γ -ray flux can have contribution to the IceCube observed events. For this purpose, the γ -ray data from *Fermi* and optical/UV/X-ray data from Swift UVOT/XRT observations of PKS 0502+049 in 2008-2018 have been analyzed. In the γ -ray band the source showed several bright periods. The maximum flux of $(4.10 \pm 0.75) \times 10^{-6} \text{ photon cm}^{-2} \text{ s}^{-1}$ integrated above 100 MeV was observed on MJD 56909.5 within 4.81 hours. During the highest flux, the apparent isotropic γ -ray luminosity is $L_\gamma \simeq 4.72 \times 10^{49} \text{ erg s}^{-1}$ (using a distance of $d_L \simeq 6269.5 \text{ Mpc}$) which corresponds to $L_{em,\gamma} = L_\gamma / 2\delta^2 \simeq 5.90 \times 10^{46} \text{ erg s}^{-1}$ (when $\delta = 20$) total power emitted in the γ -ray band in the proper frame of the jet. The γ -ray photon index varies as well, being very soft during the low states while significantly hardening in the bright periods, the hardest one being $\Gamma = 1.82 \pm 0.14$. In the X-ray band, the flux is of the order of a few times $10^{-12} \text{ erg cm}^{-2} \text{ s}^{-1}$ but with a hard photon index $\simeq 1.2 - 1.6$, unusual for FSRQs. The X-ray flux variation cannot be tested, as there are only few observations; however, an evidence of flux increasing

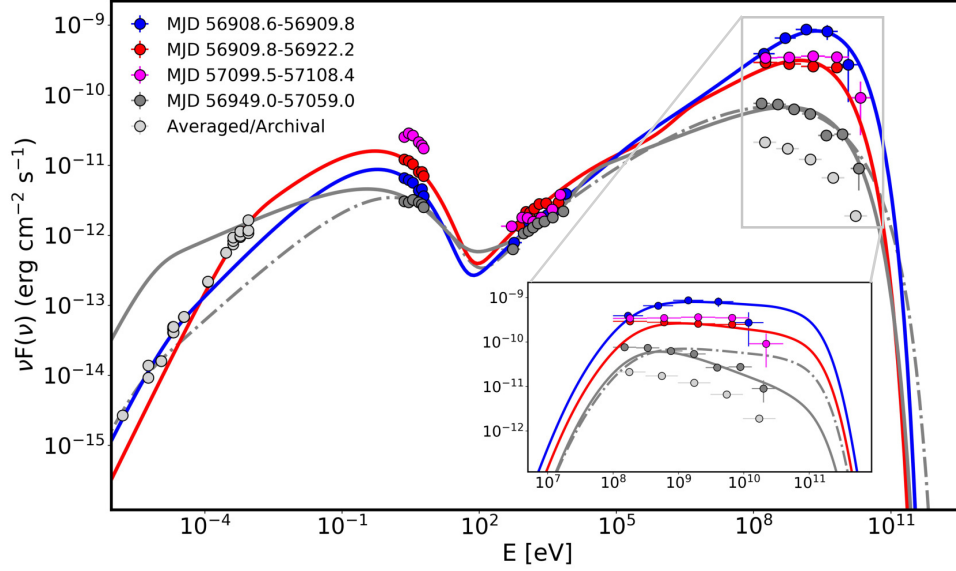


Figure 4.3 The SEDs of PKS 0502+049 during the IceCube observational window (P0; gray) and active states P1 (blue), P2 (red) and P3 (magenta). The averaged γ -ray spectrum during the considered 9 years and the archival low energy data from ASI science data center are shown in light gray. Gray, blue and red solid lines show the models when inverse Compton scattering of synchrotron (SSC) and torus (EIC) photons are considered, while the gray dot-dashed line is the fitting only with the SSC component. The model fit parameters are given in Table 4.3. The inset shows the γ -ray spectra from pp interactions where the solid lines are the modeling when the cut-off energy in the proton spectrum is fixed to 10 PeV and the gray dot-dashed line is the case when the hard spectrum of protons is considered. The axes are the same as in the main plot. All models have been corrected for $\gamma\gamma$ absorption by the extragalactic background light using the model of [54].

around the γ -ray flares can be seen. Similar tendency is present also in the optical/UV data obtained by Swift UVOT.

The γ -ray spectra when VHE neutrinos were observed as well as during the γ -ray active periods were obtained. The curved γ -ray emission spectrum during MJD 56949-57059 is better explained by a power-law model ($\sim E^{-2.07}$) with a cutoff at $E_{cut} = 8.50 \pm 2.06$ GeV. This implies the presence of a cut-off in the energy distribution of the parent population of particles responsible for the emission, so the HE processes were not dominant/efficient in the jet of PKS 0502+049 when the neutrinos were observed by IceCube. In this period, the emission from TXS 0506+056 was not dominating in the lower γ -ray band but there is an indication of a hard emission component in the higher-energy γ -rays [119], showing that most likely there was an efficient contribution from the VHE particles. When the active periods before and after the neutrinos observation window are considered, the γ -ray emission from PKS 0502+049 appears with a very hard γ -ray photon index of ≤ 2.0 . This shows even if there are certain periods when the jet of PKS 0502+049 was in a favorable state for HE and VHE γ -ray emissions, it seems not to be the case when neutrinos were observed.

Nearly symmetric flare time profiles with the shortest flux e-folding time being $t_r = 2.00 \pm 0.35$ days are obtained for the flare around MJD 57100. The rise and decay of the flare can be explained by acceleration and cooling of electrons. For example, the cooling of electrons of $E_e = 1$ GeV within $t_d = 2.62 \pm 0.39$ day requires a magnetic field of $B \approx 0.30$ G $(\delta/20)^{-1/2} (t_{dec}/2.62 d)^{-1/2} (E_e/1 GeV)^{-1/2}$ ($t_{cooling} = \delta \times t_d = 6 \pi m_e^2 c^3 / \sigma_T B^2 E_e$) which is typical for blazars.

The multiwavelength emission from PKS 0502+049 is interpreted within leptonic and hadronic scenarios. In the hadronic interpretations, the absence of VHE γ -ray data prevents exact estimations of expected neutrino rates when $p\gamma$ scenario is considered and only quantitative limits can be imposed. In the most optimistic case, the neutrino flux predicted at 100 TeV falls below the IceCube estimated one, implying the neutrinos accompanying the observed electromagnetic emission (from X- to γ -ray bands) can not be the source of the observed neutrinos. Next, if the observed γ -rays are due to pp interactions in the dense target crossing the jet, then the energy of protons is mostly released in the GeV band allowing a straightforward measurement of the proton spectra based on the observed γ -ray data. The γ -ray data obtained during the IceCube observational window can be well explained when the energy distribution of protons is $E_p^{-2.61}$. Then, if the proton cutoff energy is at ~ 10 PeV, the maximum possible neutrino detection rate will be ~ 1.1 events.

A higher neutrino detection rate is possible when a harder power-law index of protons $\alpha_p = 2.2$ is considered; however, it strongly over-predicts the HE γ -ray data above 1 – 2 GeV. Alternatively, a significant neutrino emission is expected during the γ -ray flaring periods when $\alpha_p = 2.1 - 2.2$ and only if $E_{p,c} \geq 100$ TeV; for example, in order to have a detection rate of > 4.0 events, it is required that the hard γ -ray spectra extend at least up to $\simeq E_{c,p}/40 = 2.5$ TeV - these extreme conditions are hardly possible.

In the leptonic interpretations, the broadband spectra of PKS 0502+049 are modeled within the one-zone leptonic scenario assuming the emission is produced in the compact region ($R \leq 5.31 \times 10^{16} (\delta/20)$ cm constrained by the observed variability). When the synchrotron/SSC radiation model is considered, the observed data can be explained only when the electron energy density strongly dominates over that of the magnetic field. Instead, the data can be better explained when the inverse Compton scattering of external photons is taken into account; assuming the emitting region is outside the BLR, SSC radiation from the electron population producing the radio-to-optical emission can describe the observed X-ray data while the emission in the γ -ray band with a large Compton dominance can be explained by the IC scattering of dusty torus photons. This interpretation does not require extreme parameters unlike it does in the case of pp interaction scenario, for example, the multiwavelength SED obtained during the IceCube observations can be explained when the electron power-law index is $\alpha = 2.42 \pm 0.28$ above $E'_{min} = 12.97 \pm 7.17$ MeV and $E'_c = 2.91 \pm 0.21$ GeV and the emitting region is not far from equipartition $U_e/U_B \simeq 19.6$. Similar parameters required in the modeling of flaring states are $\alpha = 1.6 - 1.9$ and $E_c \simeq 2.5$ GeV and the magnetic field of $B = (102.9 - 235.9)$ mG with an energy density not significantly different from that of the electrons $U_e/U_B = (18 - 168)$. The estimated emitting electron parameters are supported by the currently known acceleration theories and the other parameters are physically reasonable.

In the leptonic and hadronic modeling the required energetics of the system is significantly different. For example, the estimated luminosity in the leptonic scenario varies within $L_{jet} \simeq (4.5 - 18.7) \times 10^{45} \text{ erg s}^{-1}$ comfortably below the Eddington luminosity of PKS 0502+049 ($L_{Edd} \simeq 9.15 \times 10^{46} \text{ erg s}^{-1}$ for the black hole mass of $7.53 \times 10^8 M_\odot$ [117]), while in the hadronic interpretation, the accretion should be at super-Eddington rates as the required luminosity exceeds the Eddington limit by 2 – 3 orders of magnitude. Although super-Eddington accretion rate is not rare for blazars, it imposes strong difficulties

on the hadronic interpretation.

In this paper, we attempt to investigate the origin of multi-wavelength emission from PKS 0502+049 during the observation of VHE neutrinos in 2014-2015 and of γ -ray flaring periods as well as investigate whether the neutrino emission from PKS 0502+049 can have any contribution to the events observed by IceCube. The spectra observed in all periods can be well reproduced by the leptonic models with physically reasonable parameters unlike the hadronic models which require a substantially higher jet luminosity. Even in these extreme conditions, based on the γ -ray data the expected neutrino rate can be only ~ 1.1 events. In this view, considering the required energetics and predicted spectral shapes, the nearby blazar TXS 0506+056 is a more preferred source of VHE neutrinos. The presented discussion and modeling show that the broadband emission from PKS 0502+049 is most likely of a leptonic origin, leaving TXS 0506+056 as the first extragalactic source of VHE neutrinos.

5 Investigation of the Gamma-ray Spectrum of CTA 102 During the Exceptional Flaring State in 2016-2017

5.1 Introduction

Jets are observed in many classes of astrophysical objects, ranging from active galactic nuclei (AGNs) to galactic binary systems [e.g., 51, 25]. The jets mostly likely being powered by accretion processes are among the most powerful emitters of radiation in the Universe. Undoubtedly, AGNs are one of the most representative classes of astrophysical objects where the jets can be studied in all scales. The jets in these objects are manifestation of energy release from super-massive black holes (with masses up to $10^9 M_{\odot}$) and they can extended to several hundreds of kiloparsecs and in some cases to a few megaparsecs into the space often remaining highly collimated. Now the emission from these jets can be observed not only from their innermost regions, where it is stronger, but also from extended components. For example, the emission up to the X-ray band from the extended knots or hot spots of relativistic jets are observed [e.g., 76, 140, 89], the origin of the emission being explained either by synchrotron emission [77] or by the inverse Compton (IC) scattering of either synchrotron photons [75] or cosmic microwave background (CMB) photons [145, 45, 155]. However, in some cases, the IC/CMB model has been ruled out [see 108, 109, 107, 40]. Several alternative emission models for the knots involve the radiation of protons [e.g., 31, 97, 12]. Even though the observations of knots, hot-spots and lobes carries significant information on the jet energetics and dynamics but to understand the central source and the formation and propagation of the jets, it is necessary to carry out extensive studies of their initial sub-parsec-scale region.

Observation of blazars is the best way to explore the physics of jets. Blazars are a subclass of AGNs with a dominant nonthermal emission from a jet that is closely aligned with the observer's line of sight [147]. Such a geometry leads to the relativistic Doppler amplification of the emission and the radiation appears brighter for the observer. Because of this the blazars are observed even at very high redshifts [e.g., 8]. Blazars are the most luminous and energetic objects in the known universe and are the dominant sources in the extragalactic γ -ray sky. In the High Energy (HE; > 100 MeV) γ -ray band, among the 5000 sources detected to date more than 3100 are blazars [146]. One of the most distinct features of blazars is rapid variability across the whole electromagnetic spectrum with the most dramatic and short time scale changes being observed in the γ -ray band [e.g., minute scales, 10, 63, 62, 115, 41, 127, 135, 79]. This strongly constrains the emitting region size (by the light travel considerations), suggesting the radiation comes from a compact region of the jet. Traditionally the blazars are classified based on their emission lines: flat-spectrum radio quasars (FSRQs) exhibit broad emission lines, while BL Lacs show weak or no emission lines in their optical spectra. A different classification is based on the synchrotron peak frequency (ν_p): when ν_p is in the infrared, optical, or ultraviolet/X-ray bands low synchrotron peak (LSP), intermediate synchrotron peak (ISP), and high synchrotron peak (HSP) sources are classified respectively [121, 3]. Typically FSRQs are LSP/ISP blazars, whereas, BL Lacs are mostly HSP ones.

The broadband spectral energy distribution (SED) of blazars exhibits a double peaked structure, one between the infrared and X-ray bands (low energy component) and the other above the X-ray band (HE component). It is well established that the low energy component is from the synchrotron emission of electrons in the magnetic field of the jet but the nature of HE component is less well understood. The HE component is most likely due to the IC up scattering of the low energy photons produced either inside (synchrotron self Compton (SSC), [68, 35, 105]) or outside of the jet (external inverse Compton (EIC)) [34, 69, 138]). The nature of the external photon field depends on the location of the emitting region and can be either the photons directly emitted from the disk or those reflected from the broad line region (BLR) or infrared photons emitted from the dusty torus or photons from dusty torus clouds irradiated by a spine-sheath jet when the emission region is further ($> pc$) from the central objects [39]. SSC scenario was successfully applied to model the broadband SED of BL Lacs, while the SEDs of FSRQs are better explained by EIC models. Other possible processes used to model the SEDs

of blazars invoke the acceleration and emission of jet accelerated protons. These models recently were more frequently applied to model multiwavelength and multimessenger observations of TXS 0506+056 - the first cosmic neutrino source [17, 65, 47, 91, 114, 100, 149, 131] as well as its neighboring blazar PKS 0502+049 [132].

CTA 102 is one of the bright blazars observed by Fermi Large Area Telescope (Fermi LAT) in the HE γ -ray band. Even with its large distance, $z = 1.037$, CTA 102 sometimes shows strong γ -ray outburst with a flux exceeding $10^{-5} \text{ photons cm}^{-2} \text{ s}^{-1}$. For example, on 16 December 2016 (during the prolonged γ -ray activity) within 4.31 minutes the γ -ray flux above 100 MeV was as high as $(3.55 \pm 0.55) \times 10^{-5} \text{ photons cm}^{-2} \text{ s}^{-1}$, corresponding to an isotropic γ -ray luminosity of $L_\gamma = 3.25 \times 10^{50} \text{ erg s}^{-1}$, which is among the highest luminosities so far observed in the γ -ray band [66]. In addition, [137] showed that the γ -ray flux variation time can be as short as ~ 5 minutes. The analysis of multiwavelength light curves showed correlated variations in all the observed energy bands indicating co-spatial origin of the emissions [90, 66]. The broadband emission of CTA 102 is better modeled when the photons external to the jet (infrared photons from the torus) are considered [66]. As an alternative interpretation, the ablation of a gas cloud penetrating the relativistic jet of CTA 102 was discussed to be the source of the observed emission [152, 153].

The previous studies indicated a deviation of the γ -ray spectra of CTA 102 from a power-law model at HEs [90, 66]. Such breaks have already been observed in the γ -ray spectra of several blazars which can be of different origin, varying from source to source. In principle, if the emitting region is within the BLR sharp breaks in the the γ -ray spectra are expected to be due to strong attenuation of the HE and very high energy (> 100 GeV; VHE) photons through their interaction with the optical photons. The optical depth for the interaction of several tens of GeV photons can be very large, preventing their escape from the region. So, if the break is due to the absorption, it will put a constraint on the location of the γ -ray emitting region which is crucial when modeling of the observed data. Of course, a possible break in the GeV spectra does not necessarily imply absorption due to BLR photons; such break can be also due to the underlying (radiating) electrons with energy distributions deviating from a power-law spectrum. Since the γ -ray emission is caused by the IC up-scattering of low energy photons, the shape of the γ -ray spectra is directly related to the energy distribution of accelerated electrons. Thus, the modeling of the γ -ray spectra with a break can allow to probe the highest tail of the energy distribution of underlying electrons which is formed in the

interplay between the acceleration and cooling of the particles. So, this is a powerful tool for diagnosing the physics of particles in the jets. A curvature (break), if statistically significant, contains wealth of information on the possible location of the emitting region and/or on the acceleration and cooling of the particles. In this regard CTA 102 is an ideal target considering the previous indication of deviation of its γ -ray spectrum from a power-law model and availability of a large amount of simultaneous multiwavelength data.

This paper is organized as follows. The γ -ray data analysis is presented in Section 5.2. The origin of the observed breaks is investigated in Section 5.3. In Section 5.4, the origin of multiwavelength emission is discussed for a different location of the emission region. The formation of the energy distribution of radiating electrons taking into account their acceleration and cooling is investigated in Section 5.5. The results are presented and discussed in Section 5.6 while the conclusion is summarized in Section 5.7.

5.2 Fermi LAT observations

The Fermi LAT data accumulated from 01 January 2016 to 01 April 2018, when the large-amplitude flaring activities of CTA 102 occurred, are analyzed. LAT on board the Fermi satellite is a pair-conversion telescope sensitive to HE γ -rays in the 20 MeV - 300 GeV energy range [22]. Collecting the data since 2008, it is scanning the entire sky every ~ 3 hours, thereby providing most detailed view of nonthermal HE processes occurring in the astrophysical sources. The PASS8 version of the data in the energy range between 100 MeV - 300 GeV were analyzed using Fermi LAT Science Tool version 1.0.10 with the instrument response function P8R2_SOURCE_V6. The entire data set is filtered with `gtselect` and `gtmktime` tools and only the events with a high probability of being photons `evclass=128`, `evtype=3` have been considered. The zenith angle cutoff $> 90^\circ$ is chosen to exclude atmospheric γ -rays from the Earth limb that can be a significant source of background. The data downloaded from a region defined as a circle of a 12° radius centered at the γ -ray position of CTA 102 (RA, Dec) = (338.152, 11.731) are binned within a $16.9^\circ \times 16.9^\circ$ square region with `gtbin` tool with a stereographic projection into $0.1^\circ \times 0.1^\circ$ pixels. The model file describing the region of interest is generated using the *Fermi* fourth source catalog [146] (4FGL) where the sources within $12^\circ + 5^\circ$ from the position of CTA 102 are included. The model file contains also the standard Galactic `gll_iem_v07` and isotropic

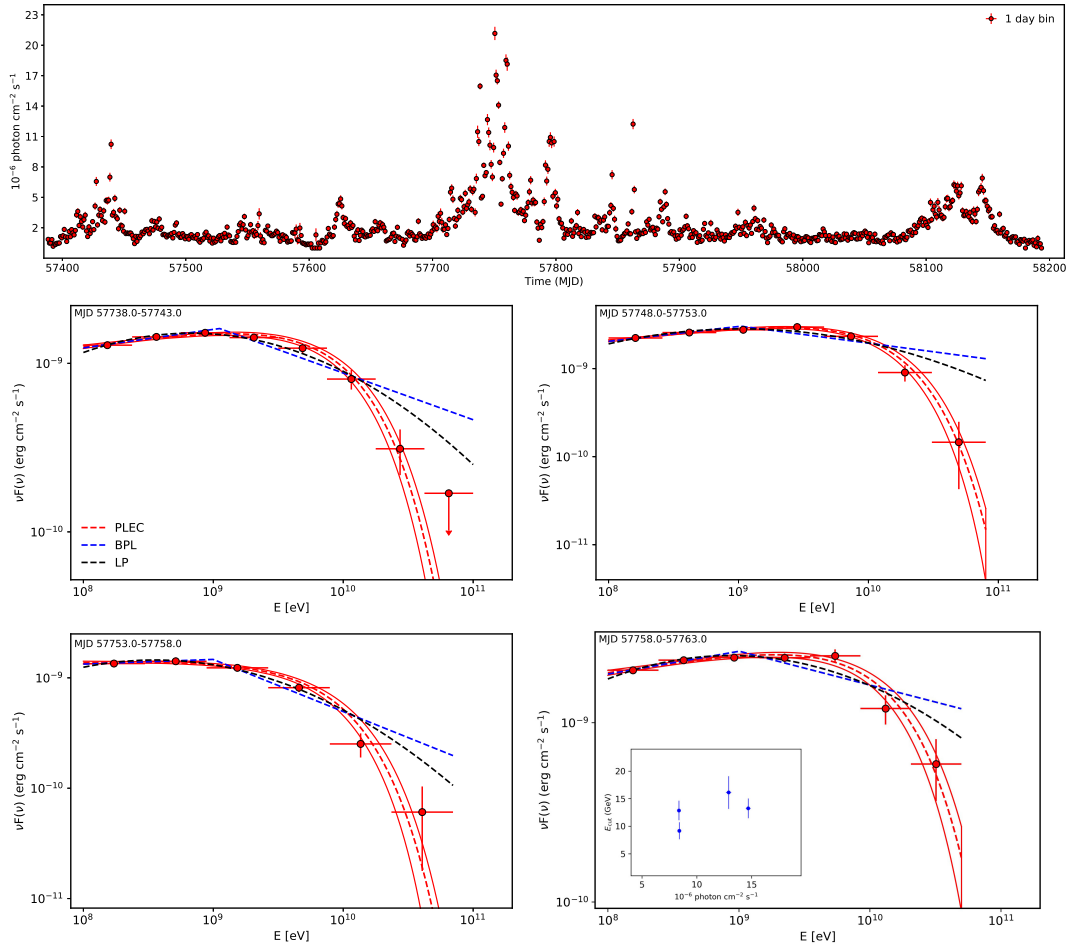


Figure 5.1 Upper Panel: The γ -ray light curve of CTA 102 with 1-day time bins from 01 January 2016 to 01 April 2018. Lower panels: The γ -ray spectra in the energy range from 100 MeV to 300 GeV for the periods which showed significant deviation from the simple power-law model. The power-law with exponential cut-off spectral model (dashed red line) with the fit uncertainties (red solid lines) are shown together with the spectral points and is compared with other adopted models (broken power-law in blue and log parabola in black). The spectral points are obtained by separately running gtlite for smaller energy intervals.

Table 5.1 The parameters of fitting with PLEC model in the periods showing deviation from the power-law model.

Period (MJD)	Γ	E_{cut} (GeV)	F_{100} (10^{-6} ph cm $^{-2}$ s $^{-1}$)	$\sqrt{2(\Delta\mathcal{L})}$
57738-57743	1.89 ± 0.02	12.86 ± 1.77	8.37 ± 0.12	10.41
57748-57753	1.84 ± 0.01	13.24 ± 1.79	14.69 ± 0.22	10.66
57753-57758	1.98 ± 0.02	9.18 ± 1.54	8.39 ± 0.14	8.30
57758-57763	1.88 ± 0.02	16.12 ± 2.98	12.89 ± 0.24	7.65

iso_P8R3_SOURCE_V2_v1 diffuse components. The normalization of background models as well as the fluxes and spectral indices of the sources within 12° are left as free parameters during the analysis. Initially, the binned likelihood analyses is applied to the full time data set adopting a log-parabola spectrum for CTA 102, however, for the light curve calculations a power-law model was used. The photon indices of all background sources were fixed to the obtained best guess values in order to reduce the uncertainties in the flux estimations in short periods. The γ -ray light curve is calculated with the unbinned likelihood analysis method implemented in the gtlike tool with the appropriate quality cuts as applied in the data selection. The γ -ray light curve with one-day binning is shown in Fig. 5.1. An interesting evolution of the γ -ray flux can be noticed: the source is in its flaring state alternatingly, with the highest flux being observed on 57750 MJD which corresponds to $(2.12 \pm 0.07) \times 10^{-5}$ photon cm $^{-2}$ s $^{-1}$ while the hardest photon index is 1.80 ± 0.06 observed on MJD 57424. This source is variable in timescales less than a day, however, for shorter periods the observed spectra will extend only up to moderate energies, preventing detailed spectral analyses. Since here the curvature in the γ -ray spectra of CTA 102 is intended to study, the periods > 1 day are considered to gather sufficient statistics. For a detailed study of the γ -ray light curve of CTA 102 in short and long time scales as well as in the multiwavelength context see [66].

The spectra of CTA 102 in 0.1-300 GeV band are investigated by detailed spectral analyses. In order to identify the periods where the spectrum significantly deviates from a simple power-law model, the data with different time binning (from 1 to 6 days) were analyzed. Yet, the time-averaged γ -ray spectrum of CTA 102 is characterized by a soft photon index with a smooth break at higher energies. So, there were further considered only the periods when

a harder photon index was observed (e.g., $\Gamma \leq 2.1$). This allows to select from the flaring states only the periods exhibiting substantially different properties as compared with those observed in the quiescent state. Then, for each period, plots of Counts/bin versus Energy and residuals between the model and the data are generated, comparing the assumed power law spectrum with the observed data. Among the selected periods, when the power-law model reasonably well explains the observed data have been excluded, so there remain only the periods where a hint of a possible deviation from a power-law model is present. Then, in order to check for a statistically significant curvature in the spectrum, an alternative fit with the following functions were considered:

a power law with an exponential cut-off (PLEC) in the form of

$$dN(E)/dE = N_0(E/E_0)^{-\Gamma} \exp(-E/E_c), \quad (5.2.1)$$

a log-parabola (LP), defined as

$$dN(E)/dE = N_0(E/E_0)^{-\alpha - \beta \ln(E/E_0)}, \quad (5.2.2)$$

and a broken power law (BPL), defined as

$$dN(E)/dE = \begin{cases} (E/E_b)^{\Gamma_1}, & \text{if } E < E_b \\ (E/E_b)^{\Gamma_2}, & \text{if } E > E_b \end{cases} \quad (5.2.3)$$

Different models are compared using a log likelihood ratio test, when the significance is estimated as twice the difference in the log-likelihoods. The spectral parameters of CTA 102 are considered as free parameters during the analyses while the photon indices of all sources within the ROI are fixed to the values obtained during the whole analysis. The best matches between the spectral models and events are obtained using an unbinned analysis method. Then, the spectrum of CTA 102 for each period was calculated by separately running glike tool for equal logarithmically-spaced energy bins.

The spectral models given in Eq. 5.2.1-5.2.2 are used to model the spectrum of CTA 102 in each single period, and the significance of the curvature was estimated by comparing each model with the power-law. Although, almost in all the considered time intervals (from one to six days) a statistically significant curvature in the γ -ray spectra was observed, the most significant it is in five-day bins. The CTA 102 spectra deviating from a simple power-law

5 Investigation of the Gamma-ray Spectrum of CTA 102 During the Exceptional Flaring State in 2016-2017

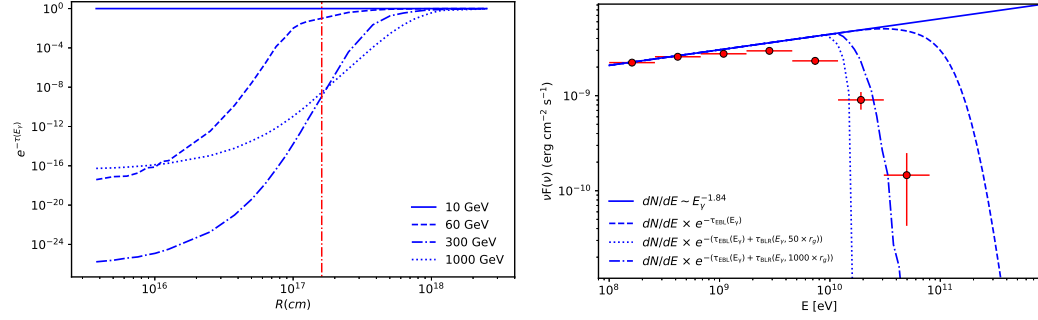


Figure 5.2 Left panel: Internal BLR absorption as a function of distance for different γ -ray energies. The red dot-dashed line shows the $R_{L\gamma\alpha}$ radius. Right panel: The reconstructed power-law model compared with the data considering external (EBL) and internal absorptions. The latter is computed assuming the emission region is at $\sim 50 r_g$ (dotted blue line) and at $\sim 1000 r_g$ (dot-dashed blue line) distances from the central source.

model with a significance exceeding 5σ are shown in the lower panel of Fig. 5.1 and the corresponding parameters are given in Table 5.1. The data fitted with PLEC (red), BPL (blue) and LP (black) models are shown. As the fitting provides only log-likelihood values the models cannot be directly compared, so the goodness of the fit (χ^2), which compares the data points with the models, is computed. This shows that the PLEC model is preferable for all the periods; other models yield a noticeably worse fit. These periods are characterized by a relatively hard photon index ($\Gamma = 1.84 - 1.98$) and a cut-off around tens of GeV which does not change significantly in different periods ($E_{\text{cut}} = 9.40 - 16.12$ GeV). The variation of E_{cut} with the flux is shown in the inset of the lower panel in Fig. 5.1. In the considered period the flux and cut-off are not varying significantly. Similar conclusion can be drawn when BPL model is considered (although it fails to explain the data observed at higher energies): the break energy varies around $E_{br} \simeq 1.0$ GeV.

5.3 Absorption of γ -rays

The curvature of the γ -ray spectrum of CTA 102, reported in the previous section, can be of different origin. In principle, it can be due to absorption, when the GeV γ -rays interact with the low energy photons (through $\gamma\gamma$ collision)

or can be related with similar steepening in the spectrum of the emitting particle distribution due to the interplay of acceleration and cooling processes. Understanding the exact nature of this steepening can help to investigate the processes taking place in the jet of CTA 102 or can help to localize the γ -ray emitting region.

The γ -rays can be absorbed either inside the source interacting with the photons reprocessed from BLR or during their propagation interacting with extragalactic background light (EBL) photons. Considering, the distance of CTA 102 ($z=1.037$), the absorption due to interaction with EBL photons is significant for energies $\geq (200 - 300)$ GeV as shown in the right panel of Fig. 5.2 (dot-dashed blue line) where the extrapolation of only the power-law component ($\sim E^{-1.84}$) observed in MJD 57748-57753 is corrected for EBL absorption using the model from [54]. Such absorption cannot explain the observed steeping of the spectrum at lower energies. In addition, if the emitting region is inside the BLR, the photons can be also effectively absorbed when interacting with the optical photons. Following the treatment of [60], the optical depth is calculated by modeling the BLR as infinitesimally thin spherical shells or thin rings. The luminosity and radius of the shells or rings are estimated using the composite quasar spectrum from the SDSS [148] in terms of $L_{H\beta}$ luminosity (which is $L_{H\beta} = (8.93 \pm 6.00) \times 10^{43} \text{ erg s}^{-1}$ for CTA 102 [110]). The absorption is dominated by $Ly\alpha$ photons at the radii 1.61×10^{17} cm (see [60], for further details) although the absorption by other lines is not negligible. The absorption by the photons directly from the accretion disk is not considered as it is significant at $\geq \text{TeV}$ γ -ray energies [55, 129, 60]. The attenuation ($e^{-\tau(E_\gamma, R)}$) strongly depends on the distance from the central object and energy of photons. For example, the plot of attenuation versus the distance is shown in Fig. 5.2 (left panel) for different distances of emitting region and for photons with energies 10, 60, 300 and 1000 GeV. The region is optically thin for 10 GeV photons (blue line in Fig. 5.2) which escape it unabsorbed. Instead, the higher-energy photons will be heavily absorbed when the emitting region is inside the BLR (dashed, dot-dashed and dotted blue lines in Fig. 5.2 left panel). The absorption decreases at larger distances making a small contribution at $> 10R_{Ly\alpha}$. Note that similar result was obtained for a different geometry of BLR [153].

The effect of attenuation due to the interaction with BLR photons in the extrapolated power-law spectrum for different distances of the emitting region is shown in Fig. 5.2 (right panel) where a factor of $(1+z)$ is taken into account

5 Investigation of the Gamma-ray Spectrum of CTA 102 During the Exceptional Flaring State in 2016-2017

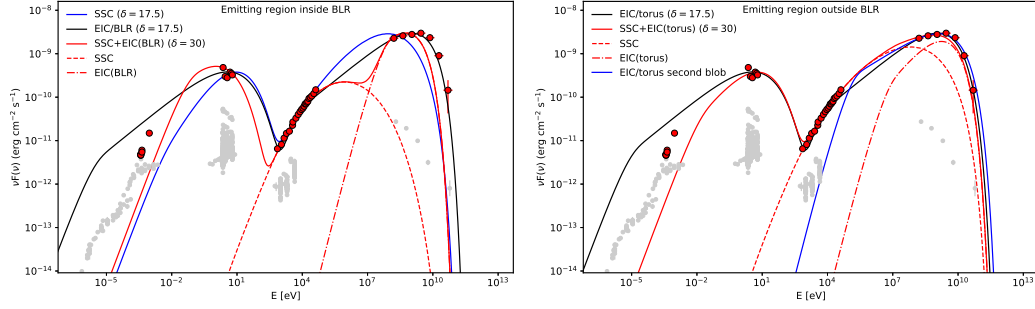


Figure 5.3 The SED of CTA 102 for the period from MJD 57748 to MJD 57753. The archival data are shown in light gray. The models are shown assuming the emitting region is inside the BLR (left panel) and outside the BLR (right panel). Different models are noted in the plot legend and the model parameters are given in the text.

for the energy as the absorption is in the galaxy frame. When the compact emitting region is at a distance of $R = 50 * r_g$ (where $r_g = 1.26 \times 10^{14} \text{ cm}$ is the gravitational radius for the CTA 102 black hole mass of $M = 8.51 \times 10^8 M_\odot$ [154]), the emitted flux will sharply decrease at energies $> 10 \text{ GeV}$ and cannot explain the observed data (dotted line in Fig. 5.2 right panel). When the region is close to the distance of BLR, $R = 1000 * r_g$, the flux drops slowly but still can not describe the observed spectra (dot-dashed blue line in Fig. 5.2 right panel): the model overproduces the flux observed around 10 GeV . For further distances, the absorption becomes less significant and the observed steepening cannot be interpreted by BLR absorption. On the other hand, the observed variability time-scales put an additional constraint on the distance of the emitting region. For example, in [126] using a 6-hour binned light curve of Fermi LAT data, the flux doubling time around MJD 57752 is 5.05 ± 0.85 hours [flare 3 in 126] which implies that the size of the emitting region is constrained by $R_\gamma \leq \delta \times c \times t_{var} / (1 + z) \simeq 2.68 \times 10^{14} \times \delta \text{ cm}$ where δ is the Doppler factor which is equal to bulk Lorentz factor for small viewing angle ($\delta \simeq \Gamma$). Using VLBA data a bulk Lorentz factor of ≥ 17.5 and a jet half opening angle of $\theta_j \leq 1^\circ.8$ were estimated for CTA 102 [98]. So, if the entire jet width is responsible for the emission, the emitting region along the jet should be at the distance of $\sim R_\gamma / \theta_j \simeq 1.49 \times 10^{17} \text{ cm}$ which is close to the upper edge of BLR. As discussed above, at these distances the absorption is relatively weak and cannot account for the observed steepening.

5.4 Origin of multiwavelength emission

Even at very close distances from the central source, the absorption due to the interaction with BLR photons cannot explain the observed steepening in the CTA 102 spectra. These breaks are most likely related with an intrinsic break in the spectrum of the radiating particles (electrons). Considering the available large amount of multiwavelength data from the observations of CTA 102, their modeling is crucial for estimating the underlying particle energy distribution which in its turn allows to study the particle acceleration and cooling processes.

The multiwavelength SED of CTA 102 is shown in Fig. 5.3 where the Swift UVOT/XRT data are from [66] for the period 3 (MJD 57752.52). For the NuStar data, the same analysis described in [66] was repeated but only the counts up to 45 keV, where the X-ray spectra of CTA 102 are above the background, were extracted. The γ -ray data are accumulated for the period from MJD 57748 to MJD 57753. The data in the mm/sub-mm band are from the ALMA catalog from the observations of bright compact radio sources in different bands between May 2011 and July 2018 [36]. From the many observations of CTA 102, only the data from the observations carried out on December 17, 18 and 29, 2016 and on January 8, 2017, which are nearly simultaneous with the studied flare, were considered. For comparison, the time averaged data from CTA 102 observations are shown in light gray, which highlights the changes observed in different energy bands.

A deviation from the power-law model has been observed in the spectra of several blazars [e.g., 5, 6, 78, 96, 128, 123, 124, 53]. The internal or external attenuation cannot be responsible for the observed steepening as demonstrated in Section 5.3. This is in agreement with the study of the spectra of 106 broad-line blazars detected in the MeV/GeV bands showing no evidence of expected BLR absorption [49]. So, the steepening might be most likely caused either by a similar feature present in the spectra of the emitting electrons or by the transition of IC scattering from Thomson to Klein-Nishina regimes. The IC scattering occurs in the Klein-Nishina regime when $E_e' > (m_e c^2)^2 / 4 / 3\epsilon_0'$. So, when the IC scattering of synchrotron photons (peaking in infrared to optical bands) or IR photons from dusty torus is considered, the IC scattering to MeV/GeV energies typically occurs in the Thomson regime. In contrast, when BLR photons are considered, the IC scattering to the same energies is in the Klein-Nishina regime. The break energy in the γ -ray spectrum naturally formed by the Klein-Nishina effects on the Compton scattering depends

on the target photon energy and is independent of δ [69, 9]. By considering different values for the target photon field, the cut-off at energies observed for CTA 102 can be reproduced by the Klein-Nishina effect. However, considering the limited information available on the BLR photons, this would be based only on inferred assumptions rather than on a real physical picture. Instead, if the break is caused by the particles and when the parameters describing the energy distribution of the particles are constrained, the physics of jets can be explored. To keep generality, during the modeling different distances for the emission region is assumed (inside and outside BLR) and all the relevant photon fields as well as the Klein-Nishina effects on the IC scattering are taken into account.

A one-zone leptonic emission scenario was used assuming that the emitting electrons are confined in a compact spherical region with a radius of $\simeq 2.68 \times 10^{14} \times \delta$ cm and magnetic field intensity of B . Due to relativistic motion of the jet, the radiation will be Doppler boosted by $\delta = \Gamma \geq 17.5$ [98] and will appear brighter for the observer. For the underlying particles a PLEC distribution within E'_{min} and E'_{max} is assumed:

$$N(E_e) = (E_e/m_e c^2)^{-\alpha} \exp(-E_e/E_c) [eV^{-1}] \quad (5.4.1)$$

considering the the total energy of electrons, $U_e = \int_{E'_{min}}^{E'_{max}} E'_e N_e(E'_e) dE'_e$, as a free parameter during the fitting. The free model parameters are estimated using Markov Chain Monte Carlo (MCMC) method which enables to derive the confidence intervals for each parameter (the application of the method and the used code are described in [133] and [66]).

5.4.1 Emitting region inside the BLR

When the emitting region is inside the BLR, the dominant photon fields which are IC up-scattering to X-ray- γ -ray bands are synchrotron photons and disc-emitted photons reflected from the BLR. The IC scattering of only synchrotron photons with ~ 1 eV peak energy on the electron population with an energy distribution with a cut at $E_{cut} \leq 1.6 \times (B/1G)^{-1/2} \times (\delta/17.5)^{-1/2}$ GeV (constrained from $E_{s,peak} \leq 1$ eV) will extend only up to (1.8 – 2) GeV which is insufficient to explain the observed data (see blue line in Fig. 5.3 left panel). Considering 10% of the disc emission is reflected from BLR with a radius of $R_{BLR} = 10^{17} (L_d/10^{45})^{0.5} = 6.3 \times 10^{17}$ cm (where $L_{disc} = 10 \times L_{BLR} \simeq$

$4.0 \times 10^{46} \text{ erg s}^{-1}$ [125]), the external photon field density in the jet frame will be $U_{BLR} = L_{BLR} \delta^2 / 4\pi R_{BLR}^2 c = 0.026 \times \delta^2 \text{ erg cm}^{-3}$. This will over-exceed the synchrotron photon density when high Doppler boosting is assumed, e.g., $\delta = 30$ which is more typical for powerful blazars. In this case, when $\alpha = 1.81 \pm 0.09$, $E'_{cut} = 0.37 \pm 0.04$ above $E'_{min} = 76.10 \pm 2.10$ MeV and the magnetic field in the emitting region is $B = 8.24 \pm 0.18$ G, the EIC peaks around GeV energies, explaining the γ -ray data, while the X-rays are due to SSC radiation (red line in Fig. 5.3 left panel). Because of the high magnetic field necessary to explain the UV and X-ray data by synchrotron/SSC processes, the electron distribution should have a lower cut-off energy ($E'_{cut} = 0.37$ GeV) which does not allow satisfactory modeling of the observed data at HEs. In this case the jet is magnetic field dominated with $U_e/U_B = 0.06$. In principle the magnetic field can be reduced by increasing the total energy of the emitting electrons, in which case the IC will overproduce the γ -ray data below ~ 1 GeV.

The required magnetic field can be decreased in an alternative model where the X-ray to γ -ray emission is due to IC up-scattering of only BLR photons (black line in Fig. 5.3 left panel). Then, when $\delta = 17.5$, the estimated magnetic field is lower, $B = 3.68 \pm 0.04$ G, and $E'_{cut} = 2.02 \pm 0.04$ GeV with $\alpha = 2.18 \pm 0.003$ allowing to model the observed data. The low-energy tail of the HE component can reproduce the X-ray data only at lower $E'_{min} = 1.1 \pm 0.01$ MeV (normally it is expected that $\gamma_{min} = E_{min}/m_e c^2$ should be close to unity [44]). However, the synchrotron emission of such low-energy electrons will overproduce the observed radio flux, but one should note that synchrotron-self absorption is not taken into account, which is significant below 4×10^{-2} eV [66].

5.4.2 Emitting region outside the BLR

When the emitting region is beyond the BLR (e.g., at $> 0.2 pc$), the IR photons from the dusty torus ($R_{IR} = 10^{18} (L_d/10^{45})^{0.5} = 6.32 \times 10^{18} \text{ cm}$ [69]) with $U_{IR} = L_{IR}/4\pi R_{IR}^2 \delta^2 = 1.59 \times 10^{-3} \times \delta^2 \text{ erg cm}^{-3}$ density will dominate over that of BLR-reflected photons which will decrease as $\sim U_{BLR}/(1 + (R/R_{BLR})^3)$ beyond R_{BLR} . In Fig. 5.3 right panel, the SED modeling when both the synchrotron and torus photons are considered is shown with red solid line (for $\delta = 30$). Again, as in the previous case, a high magnetic field $B = 2.39 \pm 0.04$ G is required (although slightly lower as the energy den-

sity of torus photons compared with BLR photons is lower), and the X-ray data can be explained by SSC mechanism. As the average energy of IR photons with $\sim 10^3$ K temperature is lower than that of BLR photons ($\sim 10^4$ K), their IC up-scattering ($\sim \delta\gamma^2(k_b T)$) can explain the observed γ -ray data when $E'_{cut} = 1.51 \pm 0.17$ GeV; the synchrotron emission of these electrons will slightly overproduce the soft X-ray data (red solid line in the right panel of Fig. 5.3).

A fit, assuming the X-ray and γ -ray data are due to IC up scattering of only torus photons, is shown in the right panel of Fig. 5.3 (black solid line). As the magnetic field is low, $B = 1.13 \pm 0.01$ G, the SSC component falls below the observed X-ray data. The power-law index of underlying electrons, $\alpha = 2.18 \pm 0.004$, is defined by joint X-ray and γ -ray data (see next section). The minimum and cut-off energies of underlying electrons are estimated to be $E'_{min} = 3.48 \pm 0.04$ MeV and $E'_{cut} = 3.60 \pm 0.09$ GeV, respectively.

Further, it is assumed that the radio-optical-X-ray and γ -ray emissions are produced in different regions (blobs). This permits to estimate the properties of emitting electrons based only on the γ -ray data, without considering the effect of the magnetic field. Such consideration is motivated by the following: i) the previous studies of this source showed that the regions outside the torus are more favorable for the γ -ray emission [66] and ii) the two-zone models were successful in explaining the bright flares of FSRQs [142]. In this case, the power-law index of the emitting electrons is $\alpha = 2.36 \pm 0.07$, much softer than in the previous cases which results in a larger cut-off energy $E'_{cut} = 5.32 \pm 0.75$ GeV. Since the X-ray data are considered as an upper limit, a larger $E'_{min} = 18.52 \pm 8.43$ MeV is obtained (red dot-dashed line in the right panel of Fig. 5.3). The jet should be very strongly particle dominated, $U_e/U_B \gg 1$ and the synchrotron emission of these electrons in the second region will not make a significant contribution to the low energy band. Such a modeling gives independent information on the particle content and distribution, as the luminosity of IC scattering depends only on N_e as distinct from the synchrotron or SSC components when the luminosity depends on the product of B^2 and N_e . Therefore, this provides straightforward information on the jet-accelerated particles.

The results obtained above do not significantly differ from those obtained in the previous studies of CTA 102 within one-zone leptonic scenarios [e.g., 126, 66]. However, it is impossible to compare the obtained parameters directly because different values of emitting region size, Doppler boosting, etc. were used in the mentioned studies. The change in the initial set of the model

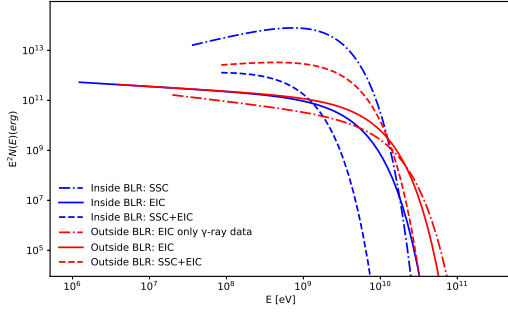


Figure 5.4 The energy distribution of the electrons for the models presented in Fig. 5.3 obtained by MCMC modeling of the observed data.

parameters impacts the estimation of other free parameters of the model. Also, the SED considered and modeled here differs from the previously modeled ones and for different periods the model parameters might vary.

5.5 Particle Acceleration and Energy losses

One of the effective ways to study the physics of the jets is through the modeling of their multiwavelength emission spectra. The applied models can reproduce/explain the data observed in a short time period which is not enough for understanding the global processes occurring in jets given the extremely variable character of their emission. However, any model trying to reproduce the transfer of the radiative output along the jet propagation should be able to explain single snapshots of the SEDs. The SED discussed here is important as the curvature in the γ -ray spectrum is most likely related with the similar feature in the emitting electron distribution, giving a chance to explore the particle acceleration and cooling mechanisms.

The electron energy distributions given by Eq. 5.4.1 that can explain the observed broadband emission of CTA 102 are shown in Fig. 5.4. The free model parameters (U_e , B , α and E'_c) were extracted straightforwardly from the observed data using the MCMC method. In order to investigate the conditions for the formation of the electron energy distribution a detailed simulation of both acceleration of particles and treatment of temporal evolution of electrons taking into account relevant energy losses (e.g, solving the kinetic equation) are required [e.g., 48]. Anyway, this is beyond the scope of this paper. Based

on the estimated parameters, here an attempt is made to put only quantitative constraints on the physical processes at work in the jet of CTA 102.

It is widely discussed that one of the most efficient mechanisms for energizing the particles in the relativistic jets of blazars is the first-order Fermi acceleration (diffuse shock acceleration [DSA]) [95, 59, 141]. A distinctive feature of this acceleration process (both for relativistic and non-relativistic shocks) is that the resulting particle energy distribution takes a power-law form ($E_e^{-\alpha}$) [57]. Under dominant radiative cooling and/or a decreasing chance for HE particles to cross the shock front a large number of times, the HE tail of the electron energy distribution steepens forming a power-law with an exponential cut-off distribution. So, the investigation of α and E'_c parameters can shed a light on the physics of the jet.

5.5.1 High energy cut-off in the electron spectrum

The HE tail of electron distribution is defined by the cooling of emitting particles which in its turn strongly depends on the location of the emitting region. For example, when the emitting region is within the BLR having a higher density, the particle cooling is more efficient and they do not reach higher energies as compared to the case when the emitting region is outside the BLR (see Fig. 5.4). The cutoff electron energy is constrained by two conditions: i) the particles are not accelerated beyond the energies when the cooling and acceleration times are equal, and ii) the particles will not continue to accelerate beyond the energies permitted by the physical size of the emitting zone: E_c is determined as the smaller of these limiting values.

When the acceleration and cooling times are of the same order, the macroscopic parameters of the jet plasma start to play a crucial role and basically they are defining the formed spectrum of emitting electrons. In the collisionless shock the non-thermal particles are gaining energy by scattering between turbulence in the upstream and downstream of the plasma. The corresponding time for diffuse shock acceleration would be [57, 130]

$$t_{acc} \simeq \eta_0 \left(\frac{p}{p_1} \right)^{\alpha_{diff}-1} \frac{m_e c \gamma'_e}{eB} \left(\frac{c}{u} \right)^2 \quad (5.5.1)$$

where p is the particle momentum, α_{diff} is the diffusion index, $\eta \sim p^{\alpha_{diff}-1}$ characterizes the diffusion ($\eta = 1$ corresponds to Bohm limit), $u \sim c$ is the

shock speed and $\gamma'_e = E'_e/m_e c^2$. Balancing this acceleration time with the electron cooling time defined as

$$t_{cool} = \frac{3 m_e c (1+z)}{4\sigma_T u'_{tot} \gamma'_e} \quad (5.5.2)$$

where $u'_{tot} = u_B + u_{SSC} + u_{IR/BLR}$ and introducing cooling parameter ϵ_{syn} defined as ratio of the luminosity of low energy component to the total luminosity, $L_{low}/(L_{low} + L_\gamma)$, [23] showed that the cutoff energy of the accelerated electrons scales with the magnetic field as $\gamma'_c \simeq \sqrt{2\mathcal{E}_s(\alpha_{diff})/3} (6 \times 10^{15}/(\eta_0 B))^{1/(1+\alpha_{diff})}$

where $\mathcal{E}_s(\alpha_{diff}) \simeq 3/2 (9\epsilon_{syn}/4)^{2/(1+\alpha_{diff})}$ (assuming $u \sim c$). Through this equation α_{diff} and η_0 are connected as $\eta_0 \simeq 1.35 \times 10^{16} \epsilon_{syn} B^{-1} \gamma_c^{-(\alpha_{diff}+1)}$ so when the magnetic field in the jet and the cutoff energy are known (e.g., from the multiwavelength data modeling) these parameters can be constrained. For CTA 102, when the emitting region is outside the BLR and the multiwavelength emission is described by synchrotron/SSC+EIC process then $B = 2.39 \pm 0.04$ G and $E'_c = 1.51 \pm 0.17$ GeV ($\gamma_c \simeq 3. \times 10^3$). For a fixed magnetic field and cutoff energy, η_0 scales inversely with α_{diff} , e.g., for Bohm type diffusion ($\alpha_{diff} = 1$) an unrealistically large $\eta_0 \simeq 10^7$ is needed (considering $\epsilon_{syn} = 0.14$). More relaxed parameters are obtained when $\alpha_{diff} > 2$: $\eta_0 \simeq 3 \times 10^4$ for $\alpha_{diff} = 2$ and $\eta_0 \simeq 10$ for $\alpha_{diff} = 3.0$. Similarly, when the data are modeled by EIC of BLR photons, when $\alpha_{diff} = 2.0$ then η_0 is 8×10^3 and η is 2.1 when $\alpha_{diff} = 3$. These parameters indicate diffusion away from the Bohm limit with a stronger dependence of the mean free path on the momentum ($\sim p^2$). Larger value of η_0 implies that turbulence levels are gradually decreasing going farther from the shock. Similar values were obtained in the modeling of multiwavelength emission from BL Lacerte and AO 0235+164 when the DSA of particles was treated with detailed Monte Carlo simulations [23], and $\eta_0 = 10^5$ was used to reproduce the broadband SED of Mrk 421 [85].

When the dynamic time scales of the system are shorter than the acceleration times, the cutoff determined from $t_{dyn} = t_{cool}$ corresponds to $\gamma'_c = 3 m_e c (1+z)/4\sigma_T u'_{tot} t_{dyn}$. If the observed γ -rays are produced in a separate region under the dominant IC cooling of torus photons, the cutoff will be $\gamma'_c = 3 \pi m_e c^2 (1+z) R_{IR}^2 / \sigma_T \eta_{IR} \delta^2 L_{disc} t_{dyn}$. For the variability time of the order of 5.05 ± 0.85 hours, the cut-off should be at $E'_e = 3.62$ GeV which is

similar to the value estimated during the fit. This shows that the curvature in the electron spectrum might also come from a limitation from the acceleration zone.

5.5.2 Power-law index of emitting electrons

The power-law index of the emitting electrons is simulation-dependent and is strictly defined by the plasma parameters. Alternatively, it can be obtained through the modeling of the observed photon spectra, in some cases analytically as well. When the HE component is interpreted by IC up-scattering of the external photon field, the particle photon index is defined by $\alpha = 2\Gamma_{\gamma/X-ray} - 1$ [e.g., 72]. In the case of CTA 102 both X-ray and γ -ray data are defining the photon index ($\alpha_{\gamma/X-ray}$) which can be obtained by fitting with a power-law function ($\sim (E/100 \text{ eV})^{-\Gamma_{\gamma/X-ray}}$). As for the BLR and torus photons IC scattering near the minimum energy of electrons (γ_{min} close to unity) is around $\sim (0.5 - 0.7)$ keV and above ~ 1 GeV the γ -ray spectrum steepens, only the data observed between ~ 0.7 keV and ~ 1 GeV are considered. The fit results in $\Gamma_{\gamma/X-ray} = 1.60 \pm 0.01$, so α should be around 2.2 which matches well with the estimated value of 2.18. In the case of SSC+EIC scenario, the power-law index is mostly but not entirely defined by fitting the SSC component to X-ray data with a slope of 1.32. The SSC component can explain the X-ray data when assuming a hard ~ 1.6 index for electron distribution but the EIC of these electrons will be steeper in the MeV/GeV band which is in disagreement with the observed data. The modeling resulted in a slightly different but still a hard spectrum for the electrons $\alpha = (1.7 - 1.8)$.

From the standpoint of shock acceleration theories the electron indexes discussed above can be easily formed under reasonable physical conditions. The DSA of particles establishes a power-law distribution of electrons with an index depending only on the shock velocity compression ratio ($\alpha = (r + 2)/(r - 1)$) [30, 32, 86]. In the case of non-relativistic shocks with a large sonic Mach number $r = 4$, so that the well known E^{-2} spectrum will be formed. When relativistic shocks are considered the picture is changed because the assumptions made in deriving the spatial diffusion equation are no longer valid and the index is defined by the shock speed and also depends on the nature of particle scattering. For a test particle in the parallel relativistic shocks the particles will be distributed by a universal power-law index of -2.23 [94, 58, 29]. However, power-law indexes varying from very hard (-1)

to very steep are possible, depending on the nature and magnitude of turbulence, shock speed and shock field obliquity [141]. One of the best ways for studying the DSA of particles is through Monte Carlo simulations (although some analytical approaches were applied as well) making a detailed treatment of the shock speed, particle scattering, etc., which is beyond the scope of the current paper. The obtained power-law indexes from 1.8 to 2.18 are well within the values discussed for shock acceleration theories to date.

5.6 Results and Discussion

The distinct blazar variability in almost all wavebands makes them ideal targets for exploring the particle acceleration and emission processes. Due to the processes causing the flares, the spectra of the sources sometimes exhibit dramatic changes in both amplitude and spectrum. So, the multiwavelength observations in these periods and their modeling can significantly help to infer/understand the physical processes at work in relativistic jets.

The CTA 102 blazar is one of the brightest γ -ray emitters in the extragalactic sky. The source is frequently in a flaring state with the most dramatic variability being demonstrated in the γ -ray band. The source showed a prolonged activity in 2016-2017 when the observed daily highest flux was $(2.12 \pm 0.07) \times 10^{-5} \text{ photon cm}^{-2} \text{ s}^{-1}$ corresponding to $\sim 2.02 \times 10^{49} \text{ erg s}^{-1}$ luminosity. The γ -ray flux in the proper frame of the jet is $L_\gamma = 3.3 \times 10^{46} \text{ erg s}^{-1}$ implying that an energy much higher than $2.8 \times 10^{51} \text{ erg}$ ($> t_{1 \text{ day}} \times L_\gamma$) should be released in the form of magnetic field and particles in order to explain the γ -ray emission.

The time-averaged γ -ray spectrum of CTA 102 is best described by a log-parabola model with $\alpha = 2.26$ and $\beta = 0.1$ while in short time scales a substantial harder emission, $\Gamma < 2.0$, with a spectrum curving at HEs is observed. Such periods were identified in the light curves with bins from 1 to 6 days. Among many periods with a hint of curvature, at least in four of them the γ -ray data are statistically significantly better ($> 7\sigma$) described by a power-law with an exponential cut-off. All these periods were during MJD 57738-57763 when the source was in a high γ -ray flaring state. During these periods the cut-off energy (9.0-16.0 GeV) was relatively stable implying that it could be due to a generic feature of the process at work in the jet of CTA 102. This cut-off is somewhat different than that observed in the time-averaged spectrum of CTA 102 and is clearly related with its flaring activity. External

absorption can be ruled out as it is significant only for the energies above 100-200 GeV for the distance of CTA 102. Internal absorption cannot account for the observed curvature as well: when the emitting region is very deep inside BLR (e.g., $\sim 50r_g$) the spectrum steepens quickly, in disagreement with the observed data, while for larger distances (e.g., $\sim 1000r_g$) the slow drop of the flux overproduces the data observed around 10 GeV. On the other hand, the observed variability time as well as the estimated bulk Lorentz factor and the jet half opening angle put a constraint on the location of the γ -ray emitting region: it should be around the upper edge or outside the BLR region. The curvature observed in the γ -ray band is most likely due to a break/cut-off in the spectrum of radiating particles.

The broadband SED of CTA 102 was modeled considering the jet dissipation occurs close (within BLR) or far from (outside BLR) the central source. The synchrotron, BLR reflected and torus photons were considered to explain the HE component in the SED of CTA 102. The free model parameters were estimated using the MCMC method. The observed X-ray data corresponding to the low-energy tail of the IC component limits the emitting electron maximum energy and the SSC component can reach only 1 – 2 GeV, not allowing to model the observed data. When the jet plasma moves with a bulk Lorentz factor of $\Gamma = \delta = 30$, the density of BLR and torus photons is comparable with or dominating over the magnetic field energy density and their IC scattering can make a significant contribution in the γ -ray band. Since their average energy in the jet frame exceeds that of synchrotron photons (peaking around 1 eV), the EIC component will extend beyond SSC and can explain the data above GeV. The combined SSC+EIC model can explain the observed data when the emitting electrons are distributed with a hard power-law index of $\simeq (1.7 - 1.8)$. On the contrary, if the jet of CTA 102 is strongly particle dominated ($U_e/U_B \simeq (10^2 - 7 \times 10^3)$) (depressing the SSC component) the IC up-scattering of only BLR or torus photons can explain the X-ray and γ -ray data if the electron distribution with ~ 2.2 index extends up to $E_c = 2.02 \pm 0.04$ GeV and $E_c = 3.60 \pm 0.09$ GeV, respectively. The total jet energy ($L_{jet} = L_B + L_e$ where $L_B = \pi c R_b^2 \Gamma^2 U_B$ and $L_e = \pi c R_b^2 \Gamma^2 U_e$) varies within $(0.04 - 2.3) \times 10^{47} \text{ erg s}^{-1}$ being of the same order or less than the Eddington accretion power for the black hole mass in CTA 102. When the γ -rays are produced in a separate region, the power-law index of the electrons (2.36 ± 0.07) and the cut-off energy (5.32 ± 0.75 GeV) are well constrained by the γ -ray data, independent of the magnetic field.

The estimated parameters of the electrons provided important information on the particle acceleration in the jet of CTA 102. The power-law index of electrons directly estimated from the X-ray or γ -ray data varies from 1.6 to 2.3- values well achievable by DSA of particles. These values cannot be directly used to put a constraint on the properties of the shock due to the complex character of the acceleration process; it can be done only under several assumptions on the unknown parameters. However, the power-law index of electron distribution capable of explaining the data is physically realistic and it can be formed in standard relativistic shocks. On the other hand, the constraint on the cutoff of the electron distribution provides a crucial information on the diffusion of particles: from the balance of acceleration and cooling times the diffusion index should be $\alpha_{diff} > 2.0$ with $\eta > 10^4$ implying that in the acceleration zone of the CTA 102jet the particle diffusion must be well removed from the Bohm limit ($\eta = 1$ and $\alpha_{diff} = 1$). These parameters show that the physical environment in the jet of CTA 102should have a lower-level turbulence at large distances from the shocks, which results in longer diffusive mean free paths for larger momenta. These conditions are not physically unrealistic and can be formed under certain circumstances. For further discussion see [23] and references therein.

5.7 Conclusions

The origin of the curvature in the γ -ray spectra of CTA 102is investigated. During bright γ -ray flaring of CTA 102its emission spectrum hardened, steepening above ~ 10 GeV and the data are better ($> 7\sigma$) described by a power-law with exponential cut-off model. The estimated cut-off energy remains relatively unchanged (taking into account the uncertainties).

The modeling of the SED of CTA 102allowed to constrain the free model parameters with their uncertainties, which in its turn provided information on the particle acceleration. The electron spectrum can be easily formed by diffusive shock acceleration but it is required that the diffusion occurs well beyond the Bohm limit. The prolonged γ -ray flaring activity of the source in 2016-2017 could be in principle due to such changes in the jet of CTA 102.

Here a single snapshot of the SED of CTA 102is modeled, providing a valuable information on particle acceleration and cooling processes. Observation, identification and modeling of different flaring periods characterized by a curvature in the γ -ray spectrum can eventually help to draw a clear picture

*5 Investigation of the Gamma-ray Spectrum of CTA 102 During the
Exceptional Flaring State in 2016-2017*

of the global processes taking place in the blazar jets.

Bibliography

- [1] M. G. Aartsen, R. Abbasi, Y. Abdou, M. Ackermann, J. Adams, J. A. Aguilar, M. Ahlers, D. Altmann, J. Auffenberg, X. Bai, and et al. First Observation of PeV-Energy Neutrinos with IceCube. *Physical Review Letters*, 111(2):021103, July 2013.
- [2] M. G. Aartsen, K. Abraham, M. Ackermann, and et al. All-sky Search for Time-integrated Neutrino Emission from Astrophysical Sources with 7 yr of IceCube Data. *ApJ*, 835:151, February 2017.
- [3] A. A. Abdo, M. Ackermann, I. Agudo, M. Ajello, H. D. Aller, M. F. Aller, E. Angelakis, A. A. Arkharov, M. Axelsson, U. Bach, L. Baldini, J. Ballet, G. Barbiellini, D. Bastieri, B. M. Baughman, K. Bechtol, R. Bellazzini, E. Benitez, A. Berdyugin, B. Berenji, R. D. Blandford, E. D. Bloom, M. Boettcher, E. Bonamente, A. W. Borgland, J. Bregeon, A. Brez, M. Brigida, P. Bruel, T. H. Burnett, D. Burrows, S. Buson, G. A. Caliandro, L. Calzoletti, R. A. Cameron, M. Capalbi, P. A. Caraveo, D. Carosati, J. M. Casandjian, E. Cavazzuti, C. Cecchi, Ö. Çelik, E. Charles, S. Chaty, A. Chekhtman, W. P. Chen, J. Chiang, G. Chincarini, S. Ciprini, R. Claus, J. Cohen-Tanugi, S. Colafrancesco, L. R. Cominsky, J. Conrad, L. Costamante, S. Cutini, F. D'Ammando, R. Deitrick, V. D'Elia, C. D. Dermer, A. de Angelis, F. de Palma, S. W. Digel, I. Donnarumma, E. do Couto e Silva, P. S. Drell, R. Dubois, D. Dultzin, D. Dumora, A. Falcone, C. Farnier, C. Favuzzi, S. J. Fegan, W. B. Focke, E. Forné, P. Fortin, M. Frailis, L. Fuhrmann, Y. Fukazawa, S. Funk, P. Fusco, J. L. Gómez, F. Gargano, D. Gasparrini, N. Gehrels, S. Germani, B. Giebels, N. Giglietto, P. Giommi, F. Giordano, A. Giuliani, T. Glanzman, G. Godfrey, I. A. Grenier, C. Gronwall, J. E. Grove, L. Guillemot, S. Guiriec, M. A. Gurwell, D. Hadasch, Y. Hanabata, A. K. Harding, M. Hayashida, E. Hays, S. E. Healey, J. Heidt,

D. Hiriart, D. Horan, E. A. Hoversten, R. E. Hughes, R. Itoh, M. S. Jackson, G. Jóhannesson, A. S. Johnson, W. N. Johnson, S. G. Jorstad, M. Kadler, T. Kamae, H. Katagiri, J. Kataoka, N. Kawai, J. Kennea, M. Kerr, G. Kimeridze, J. Knödlseider, M. L. Kocian, E. N. Kopatskaya, E. Koptelova, T. S. Konstantinova, Y. Y. Kovalev, Yu. A. Kovalev, O. M. Kurtanidze, M. Kuss, J. Lande, V. M. Larionov, L. Latronico, P. Leto, E. Lindfors, F. Longo, F. Loparco, B. Lott, M. N. Lovellette, P. Lubrano, G. M. Madejski, A. Makeev, P. Marchegiani, A. P. Marscher, F. Marshall, W. Max-Moerbeck, M. N. Mazziotta, W. McConville, J. E. McEnery, C. Meurer, P. F. Michelson, W. Mitthumsiri, T. Mizuno, A. A. Moiseev, C. Monte, M. E. Monzani, A. Morselli, I. V. Moskalenko, S. Murgia, I. Nestoras, K. Nilsson, N. A. Nizhelsky, P. L. Nolan, J. P. Norris, E. Nuss, T. Ohsugi, R. Ojha, N. Omodei, E. Orlando, J. F. Ormes, J. Osborne, M. Ozaki, L. Paciani, P. Padovani, C. Pagani, K. Page, D. Paneque, J. H. Panetta, D. Parent, M. Pasanen, V. Pavlidou, V. Pelassa, M. Pepe, M. Perri, M. Pesce-Rollins, S. Piranomonte, F. Piron, C. Pittori, T. A. Porter, S. Puccetti, F. Rahoui, S. Rainò, C. Raiteri, R. Rando, M. Razzano, A. Reimer, O. Reimer, T. Reposeur, J. L. Richards, S. Ritz, L. S. Rochester, A. Y. Rodriguez, R. W. Romani, J. A. Ros, M. Roth, P. Roustazadeh, F. Ryde, H. F. W. Sadrozinski, A. Sadun, D. Sanchez, A. Sander, P. M. Saz Parkinson, J. D. Scargle, A. Sellerholm, C. Sgrò, M. S. Shaw, L. A. Sigua, E. J. Siskind, D. A. Smith, P. D. Smith, G. Spandre, P. Spinelli, J. L. Starck, M. Stevenson, G. Stratta, M. S. Strickman, D. J. Suson, H. Tajima, H. Takahashi, T. Takahashi, L. O. Takalo, T. Tanaka, J. B. Thayer, J. G. Thayer, D. J. Thompson, L. Tibaldo, D. F. Torres, G. Tosti, A. Tramacere, Y. Uchiyama, T. L. Usher, V. Vasileiou, F. Verrecchia, N. Vilchez, M. Villata, V. Vitale, A. P. Waite, P. Wang, B. L. Winer, K. S. Wood, T. Ylinen, J. A. Zensus, G. V. Zhekanis, and M. Ziegler.

The Spectral Energy Distribution of Fermi Bright Blazars.
ApJ, 716(1):30–70, Jun 2010.

- [4] A. A. Abdo, M. Ackermann, M. Ajello, , and et al.
Gamma-ray Light Curves and Variability of Bright Fermi-detected Blazars.
ApJ, 722:520–542, October 2010.

- [5] A. A. Abdo, M. Ackermann, M. Ajello, W. B. Atwood, M. Axelsson, L. Baldini, J. Ballet, G. Barbiellini, D. Bastieri, M. Battelino, B. M. Baughman, K. Bechtol, R. Bellazzini, B. Berenji, R. D. Blandford, E. D. Bloom, E. Bonamente, A. W. Borgland, A. Bouvier, J. Bregeon, A. Brez, M. Brigida, P. Bruel, T. H. Burnett, G. A. Caliandro, R. A. Cameron, P. A. Caraveo, J. M. Casandjian, E. Cavazzuti, C. Cecchi, E. Charles, S. Chaty, A. Chekhtman, C. C. Cheung, J. Chiang, S. Ciprini, R. Claus, J. Cohen-Tanugi, L. R. Cominsky, J. Conrad, L. Costamante, S. Cutini, C. D. Dermer, A. de Angelis, F. de Palma, S. W. Digel, E. do Couto e. Silva, D. Donato, P. S. Drell, R. Dubois, D. Dumora, C. Farnier, C. Favuzzi, W. B. Focke, L. Foschini, M. Frailis, L. Fuhrmann, Y. Fukazawa, S. Funk, P. Fusco, F. Gargano, D. Gasparrini, N. Gehrels, S. Germani, B. Giebels, N. Giglietto, P. Giommi, F. Giordano, T. Glanzman, G. Godfrey, I. A. Grenier, M. H. Grondin, J. E. Grove, L. Guillemot, S. Guiriec, Y. Hanabata, A. K. Harding, R. C. Hartman, M. Hayashida, E. Hays, R. E. Hughes, G. Jóhannesson, A. S. Johnson, R. P. Johnson, W. N. Johnson, T. Kamae, H. Katagiri, J. Kataoka, N. Kawai, M. Kerr, J. Knödseder, M. L. Kocian, F. Kuehn, M. Kuss, L. Latronico, S. H. Lee, M. Lemoine-Goumard, F. Longo, F. Loparco, B. Lott, M. N. Lovellette, P. Lubrano, G. M. Madejski, A. Makeev, E. Massaro, M. N. Mazziotta, J. E. McEnery, S. McGlynn, C. Meurer, P. F. Michelson, W. Mitthumsiri, T. Mizuno, A. A. Moiseev, C. Monte, M. E. Monzani, A. Morselli, I. V. Moskalenko, S. Murgia, P. L. Nolan, J. P. Norris, E. Nuss, T. Ohsugi, N. Omodei, E. Orlando, J. F. Ormes, D. Paneque, J. H. Panetta, D. Parent, V. Pelassa, M. Pepe, M. Pesce-Rollins, F. Piron, T. A. Porter, S. Rainò, R. Rando, M. Razzano, A. Reimer, O. Reimer, T. Reposeur, L. C. Reyes, S. Ritz, L. S. Rochester, A. Y. Rodriguez, F. Rahoui, F. Ryde, H. F. W. Sadrozinski, R. Sambruna, D. Sanchez, A. Sander, P. M. Saz Parkinson, C. Sgrò, M. S. Shaw, D. A. Smith, P. D. Smith, G. Spandre, P. Spinelli, J. L. Starck, M. S. Strickman, D. J. Suson, H. Tajima, H. Takahashi, T. Takahashi, T. Tanaka, J. B. Thayer, J. G. Thayer, D. J. Thompson, L. Tibaldo, D. F. Torres, G. Tosti, A. Tramacere, Y. Uchiyama, T. L. Usher, N. Vilchez, M. Villata, V. Vitale, A. P. Waite, B. L. Winer, K. S. Wood, T. Ylinen, J. A. Zensus, and M. Ziegler.

Early Fermi Gamma-ray Space Telescope Observations of the Quasar 3C 454.3.

- ApJ*, 699(1):817–823, Jul 2009.
- [6] A. A. Abdo, M. Ackermann, M. Ajello, and et al.
Spectral Properties of Bright Fermi-Detected Blazars in the Gamma-Ray Band.
ApJ, 710:1271–1285, February 2010.
- [7] A. U. Abeysekara, S. Archambault, A. Archer, T. Aune, A. Barnacka, W. Benbow, R. Bird, J. Biteau, J. H. Buckley, V. Bugaev, J. V. Cardenzana, M. Cerruti, X. Chen, J. L. Christiansen, L. Ciupik, M. P. Connolly, P. Coppi, W. Cui, H. J. Dickinson, J. Dumm, J. D. Eisch, M. Errando, A. Falcone, Q. Feng, J. P. Finley, H. Fleischhack, A. Flinders, P. Fortin, L. Fortson, A. Furniss, G. H. Gillanders, S. Griffin, J. Grube, G. Gyuk, M. Hütten, N. HA&Akansson, D. Hanna, J. Holder, T. B. Humensky, C. A. Johnson, P. Kaaret, P. Kar, N. Kelley-Hoskins, Y. Khassen, D. Kieda, M. Krause, F. Krennrich, S. Kumar, M. J. Lang, G. Maier, S. McArthur, A. McCann, K. Meagher, P. Moriarty, R. Mukherjee, D. Nieto, A. O’Faoláin de Bhróithe, R. A. Ong, A. N. Otte, N. Park, J. S. Perkins, A. Petrashyk, M. Pohl, A. Popkow, E. Pueschel, J. Quinn, K. Ragan, G. Ratliff, P. T. Reynolds, G. T. Richards, E. Roache, J. Rousselle, M. Santander, G. H. Sembroski, K. Shahinyan, A. W. Smith, D. Staszak, I. Telezhinsky, N. W. Todd, J. V. Tucci, J. Tyler, V. V. Vassiliev, S. Vincent, S. P. Wakely, O. M. Weiner, A. Weinstein, A. Wilhelm, D. A. Williams, B. Zitzer, VERITAS, P. S. Smith, SPOL, T. W.-S. Holoien, J. L. Prieto, C. S. Kochanek, K. Z. Stanek, B. Shappee, ASAS-SN, T. Hovatta, W. Max-Moerbeck, T. J. Pearson, R. A. Reeves, J. L. Richards, A. C. S. Readhead, OVRO, G. M. Madejski, NuSTAR, S. G. Djorgovski, A. J. Drake, M. J. Graham, A. Mahabal, and CRTS.
Gamma-Rays from the Quasar PKS 1441+25: Story of an Escape.
ApJL, 815:L22, December 2015.
- [8] M. Ackermann, M. Ajello, L. Baldini, J. Ballet, G. Barbiellini, D. Bastieri, J. Becerra Gonzalez, R. Bellazzini, E. Bissaldi, R. D. Blandford, E. D. Bloom, R. Bonino, E. Bottacini, J. Bregeon, P. Bruel, R. Buehler, S. Buson, R. A. Cameron, M. Caragiulo, P. A. Caraveo, E. Cavazzuti, C. Cecchi, C. C. Cheung, J. Chiang, G. Chiaro, S. Ciprini, J. Conrad, D. Costantin, F. Costanza, S. Cutini, F. D’Ammando, F. de Palma, R. Desiante, S. W. Digel, N. Di Lalla, M. Di Mauro, L. Di Venere,

A. Domínguez, P. S. Drell, C. Favuzzi, S. J. Fegan, E. C. Ferrara, J. Finke, W. B. Focke, Y. Fukazawa, S. Funk, P. Fusco, F. Gargano, D. Gasparri, N. Giglietto, F. Giordano, M. Giroletti, D. Green, I. A. Grenier, L. Guillemot, S. Guiriec, D. H. Hartmann, E. Hays, D. Horan, T. Jogler, G. Jóhannesson, A. S. Johnson, M. Kuss, G. La Mura, S. Larsson, L. Latronico, J. Li, F. Longo, F. Loparco, M. N. Lovellette, P. Lubrano, J. D. Magill, S. Maldera, A. Manfreda, L. Marcotulli, M. N. Mazziotta, P. F. Michelson, N. Mirabal, W. Mitthumsiri, T. Mizuno, M. E. Monzani, A. Morselli, I. V. Moskalenko, M. Negro, E. Nuss, T. Ohsugi, R. Ojha, N. Omodei, M. Orienti, E. Orlando, J. F. Ormes, V. S. Paliya, D. Paneque, J. S. Perkins, M. Persic, M. Pesce-Rollins, F. Piron, T. A. Porter, G. Principe, S. Rainò, R. Rando, B. Rani, M. Razzano, S. Razzaque, A. Reimer, O. Reimer, R. W. Romani, C. Sgrò, D. Simone, E. J. Siskind, F. Spada, G. Spandre, P. Spinelli, C. S. Stalin, L. Stawarz, D. J. Suson, M. Takahashi, K. Tanaka, J. B. Thayer, D. J. Thompson, D. F. Torres, E. Torresi, G. Tosti, E. Troja, G. Vianello, and K. S. Wood.

Gamma-Ray Blazars within the First 2 Billion Years.

ApJL, 837(1):L5, Mar 2017.

- [9] M. Ackermann, M. Ajello, L. Baldini, J. Ballet, G. Barbiellini, D. Bastieri, K. Bechtol, R. Bellazzini, B. Berenji, R. D. Blandford, E. Bonamente, A. W. Borgland, J. Bregeon, M. Brigida, P. Bruel, R. Buehler, T. H. Burnett, S. Buson, G. A. Caliandro, R. A. Cameron, P. A. Caraveo, S. Carrigan, J. M. Casandjian, E. Cavazzuti, C. Cecchi, Ö. Çelik, A. Chekhtman, C. C. Cheung, J. Chiang, S. Ciprini, R. Claus, J. Cohen-Tanugi, S. Corbel, S. Cutini, F. D'Ammando, C. D. Dermer, A. de Angelis, F. de Palma, S. W. Digel, E. do Couto e Silva, P. S. Drell, R. Dubois, D. Dumora, L. Escande, C. Favuzzi, S. J. Fegan, E. C. Ferrara, L. Fuhrmann, Y. Fukazawa, P. Fusco, F. Gargano, D. Gasparri, N. Gehrels, S. Germani, B. Giebels, N. Giglietto, P. Giommi, F. Giordano, M. Giroletti, T. Glanzman, G. Godfrey, I. A. Grenier, J. E. Grove, S. Guiriec, D. Hadasch, M. Hayashida, E. Hays, G. Jóhannesson, A. S. Johnson, W. N. Johnson, T. Kamae, H. Katagiri, J. Kataoka, J. Knödseder, M. Kuss, J. Lande, S. Larsson, L. Latronico, S. H. Lee, M. Llana Garde, F. Longo, F. Loparco, B. Lott, P. Lubrano, G. M. Madejski, A. Makeev, N. Marchili, M. N. Mazziotta, J. E. McEnery, J. Mehault, P. F. Michelson, T. Mizuno,

C. Monte, M. E. Monzani, A. Morselli, I. V. Moskalenko, S. Murgia, T. Nakamori, K. Nalewajko, M. Naumann-Godo, P. L. Nolan, J. P. Norris, E. Nuss, T. Ohsugi, A. Okumura, N. Omodei, E. Orlando, J. F. Ormes, V. Pelassa, M. Pepe, M. Pesce-Rollins, F. Piron, T. A. Porter, S. Rainò, R. Rando, M. Razzano, A. Reimer, O. Reimer, L. C. Reyes, J. Ripken, S. Ritz, M. Roth, H. F. W. Sadrozinski, D. Sanchez, A. Sander, J. D. Scargle, C. Sgrò, M. Sikora, E. J. Siskind, G. Spandre, P. Spinelli, M. S. Strickman, D. J. Suson, H. Takahashi, T. Takahashi, T. Tanaka, Y. Tanaka, J. B. Thayer, J. G. Thayer, D. J. Thompson, L. Tibaldo, D. F. Torres, G. Tosti, A. Tramacere, T. L. Usher, J. Vandenbroucke, N. Vilchez, V. Vitale, A. P. Waite, P. Wang, A. E. Wehrle, B. L. Winer, Z. Yang, T. Ylinen, and M. Ziegler.

Fermi Gamma-ray Space Telescope Observations of Gamma-ray Outbursts from 3C 454.3 in 2009 December and 2010 April.
ApJ, 721(2):1383–1396, Oct 2010.

- [10] M. Ackermann, R. Anantua, and et al.
Minute-timescale >100 MeV γ -Ray Variability during the Giant Outburst of Quasar 3C 279 Observed by Fermi-LAT in 2015 June.
ApJL, 824:L20, June 2016.
- [11] F. Aharonian, A. G. Akhperjanian, A. R. Bazer-Bachi, B. Behera, M. Beilicke, W. Benbow, D. Berge, K. Bernlöhner, C. Boisson, O. Bolz, V. Borrel, T. Boutelier, I. Braun, E. Brion, A. M. Brown, R. Bühler, I. Büsching, T. Bulik, S. Carrigan, P. M. Chadwick, A. C. Clapson, L.-M. Chounet, G. Coignet, R. Cornils, L. Costamante, B. Degrange, H. J. Dickinson, A. Djannati-Ataï, W. Domainko, L. O. Drury, G. Dubus, J. Dyks, K. Egberts, D. Emmanoulopoulos, P. Espigat, C. Farnier, F. Feinstein, A. Fiasson, A. Förster, G. Fontaine, S. Funk, S. Funk, M. Füßling, Y. A. Gallant, B. Giebels, J. F. Glicenstein, B. Glück, P. Goret, C. Hadjichristidis, D. Hauser, M. Hauser, G. Heinzlmann, G. Henri, G. Hermann, J. A. Hinton, A. Hoffmann, W. Hofmann, M. Holleran, S. Hoppe, D. Horns, A. Jacholkowska, O. C. de Jager, E. Kendziorra, M. Kerschhaggl, B. Khélifi, N. Komin, K. Kosack, G. Lamanna, I. J. Latham, R. Le Gallou, A. Lemièrre, M. Lemoine-Goumard, J.-P. Lenain, T. Lohse, J. M. Martin, O. Martineau-Huynh, A. Marcowith, C. Masterson, G. Maurin, T. J. L. McComb, R. Moderski, E. Moulin, M. de Naurois,

-
- D. Nedbal, S. J. Nolan, J.-P. Olive, K. J. Orford, J. L. Osborne, M. Ostrowski, M. Panter, G. Pedalletti, G. Pelletier, P.-O. Petrucci, S. Pita, G. Pühlhofer, M. Punch, S. Ranchon, B. C. Raubenheimer, M. Raue, S. M. Rayner, M. Renaud, J. Ripken, L. Rob, L. Rolland, S. Rosier-Lees, G. Rowell, B. Rudak, J. Ruppel, V. Sahakian, A. Santangelo, L. Saugé, S. Schlenker, R. Schlickeiser, R. Schröder, U. Schwanke, S. Schwarzburg, S. Schwemmer, A. Shalchi, H. Sol, D. Spangler, Ł. Stawarz, R. Steenkamp, C. Stegmann, G. Superina, P. H. Tam, J.-P. Tavernet, R. Terrier, C. van Eldik, G. Vasileiadis, C. Venter, J. P. Vialle, P. Vincent, M. Vivier, H. J. Völk, F. Volpe, S. J. Wagner, M. Ward, and A. A. Zdziarski.
- An Exceptional Very High Energy Gamma-Ray Flare of PKS 2155-304. *ApJL*, 664:L71–L74, August 2007.
- [12] F. A. Aharonian.
Proton-synchrotron radiation of large-scale jets in active galactic nuclei. *MNRAS*, 332:215–230, May 2002.
- [13] M. Ahlers and F. Halzen.
High-energy cosmic neutrino puzzle: a review. *Reports on Progress in Physics*, 78(12):126901, December 2015.
- [14] M. L. Ahnen, S. Ansoldi, L. A. Antonelli, P. Antoranz, A. Babic, B. Banerjee, P. Bangale, U. Barres de Almeida, J. A. Barrio, W. Bednarek, and et al.
Very High Energy γ -Rays from the Universe’s Middle Age: Detection of the $z = 0.940$ Blazar PKS 1441+25 with MAGIC. *ApJL*, 815:L23, December 2015.
- [15] J. Albert, E. Aliu, H. Anderhub, P. Antoranz, A. Armada, C. Baixeras, J. A. Barrio, H. Bartko, D. Bastieri, J. K. Becker, W. Bednarek, K. Berger, C. Bigongiari, A. Biland, R. K. Bock, P. Bordas, V. Bosch-Ramon, T. Bretz, I. Britvitch, M. Camara, E. Carmona, A. Chilingarian, J. A. Coarasa, S. Commichau, J. L. Contreras, J. Cortina, M. T. Costado, V. Curtef, V. Danielyan, F. Dazzi, A. De Angelis, C. Delgado, R. de los Reyes, B. De Lotto, E. Domingo-Santamaría, D. Dorner, M. Doro, M. Errando, M. Fagiolini, D. Ferenc, E. Fernández, R. Firpo, J. Flix, M. V. Fonseca, L. Font, M. Fuchs, N. Galante, R. J. García-López, M. Garczarczyk, M. Gaug, M. Giller,

F. Goebel, D. Hakobyan, M. Hayashida, T. Hengstebeck, A. Her-
rero, D. Höhne, J. Hose, D. Hrupec, C. C. Hsu, P. Jacon, T. Jogler,
R. Kosyra, D. Kranich, R. Kritzer, A. Laille, E. Lindfors, S. Lombardi,
F. Longo, J. López, M. López, E. Lorenz, P. Majumdar, G. Maneva,
K. Mannheim, O. Mansutti, M. Mariotti, M. Martínez, D. Mazin,
C. Merck, M. Meucci, M. Meyer, J. M. Miranda, R. Mirzoyan, S. Mi-
zobuchi, A. Moralejo, D. Nieto, K. Nilsson, J. Ninkovic, E. Oña-
Wilhelmi, N. Otte, I. Oya, D. Paneque, M. Panniello, R. Paoletti, J. M.
Paredes, M. Pasanen, D. Pascoli, F. Pauss, R. Pegna, M. Persic, L. Pe-
ruzzo, A. Piccioli, E. Prandini, N. Puchades, A. Raymers, W. Rhode,
M. Ribó, J. Rico, M. Rissi, A. Robert, S. Rügamer, A. Saggion,
T. Saito, A. Sánchez, P. Sartori, V. Scalzotto, V. Scapin, R. Schmitt,
T. Schweizer, M. Shayduk, K. Shinozaki, S. N. Shore, N. Sidro, A. Sil-
lanpää, D. Sobczynska, A. Stamerra, L. S. Stark, L. Takalo, F. Tavec-
chio, P. Temnikov, D. Tesaro, M. Teshima, D. F. Torres, N. Turini,
H. Vankov, V. Vitale, R. M. Wagner, T. Wibig, W. Wittek, F. Zan-
danel, R. Zanin, and J. Zapatero.

Variable Very High Energy γ -Ray Emission from Markarian 501.
ApJ, 669:862–883, November 2007.

- [16] J. Aleksić, L. A. Antonelli, P. Antoranz, M. Backes, J. A. Barrio,
D. Bastieri, J. Becerra González, W. Bednarek, A. Berdyugin,
K. Berger, E. Bernardini, A. Biland, O. Blanch, R. K. Bock, A. Boller,
G. Bonnoli, D. Borla Tridon, I. Braun, T. Bretz, A. Cañellas, E. Car-
mona, A. Carosi, P. Colin, E. Colombo, J. L. Contreras, J. Cortina,
L. Cossio, S. Covino, F. Dazzi, A. De Angelis, E. De Cea del Pozo,
B. De Lotto, C. Delgado Mendez, A. Diago Ortega, M. Doert,
A. Domínguez, D. Dominis Prester, D. Dorner, M. Doro, D. El-
saesser, D. Ferenc, M. V. Fonseca, L. Font, C. Fruck, R. J. García
López, M. Garczarczyk, D. Garrido, G. Giavitto, N. Godinović,
D. Hadasch, D. Häfner, A. Herrero, D. Hildebrand, D. Höhne-
Mönch, J. Hose, D. Hrupec, B. Huber, T. Jogler, S. Klepser,
T. Krähenbühl, J. Krause, A. La Barbera, D. Lelas, E. Leonardo,
E. Lindfors, S. Lombardi, M. López, E. Lorenz, M. Makariev,
G. Maneva, N. Mankuzhiyil, K. Mannheim, L. Maraschi, M. Mari-
otti, M. Martínez, D. Mazin, M. Meucci, J. M. Miranda, R. Mirzoyan,
H. Miyamoto, J. Moldón, A. Moralejo, D. Nieto, K. Nilsson, R. Orito,
I. Oya, D. Paneque, R. Paoletti, S. Pardo, J. M. Paredes, S. Partini,

M. Pasanen, F. Pauss, M. A. Perez-Torres, M. Persic, L. Peruzzo, M. Pilia, J. Pochon, F. Prada, P. G. Prada Moroni, E. Prandini, I. Puljak, I. Reichardt, R. Reinthal, W. Rhode, M. Ribó, J. Rico, S. Rügamer, A. Saggion, K. Saito, T. Y. Saito, M. Salvati, K. Satalecka, V. Scalzotto, V. Scapin, C. Schultz, T. Schweizer, M. Shayduk, S. N. Shore, A. Siljanpää, J. Sitarek, D. Sobczynska, F. Spanier, S. Spiro, A. Stamerra, B. Steinke, J. Storz, N. Strah, T. Surić, L. Takalo, F. Tavecchio, P. Temnikov, T. Terzić, D. Tescaro, M. Teshima, M. Thom, O. Tibolla, D. F. Torres, A. Treves, H. Vankov, P. Vogler, R. M. Wagner, Q. Weitzel, V. Zabalza, F. Zandanel, R. Zanin, MAGIC Collaboration, Y. T. Tanaka, D. L. Wood, and S. Buson.

MAGIC Discovery of Very High Energy Emission from the FSRQ PKS 1222+21.

ApJL, 730:L8, March 2011.

- [17] S. Ansoldi, L. A. Antonelli, C. Arcaro, D. Baack, A. Babić, B. Banerjee, P. Bangale, U. Barres de Almeida, J. A. Barrio, J. Becerra González, W. Bednarek, E. Bernardini, R. C. Berse, A. Berti, J. Besenrieder, W. Bhattacharyya, C. Bigongiari, A. Biland, O. Blanch, G. Bonoli, R. Carosi, G. Ceribella, A. Chatterjee, S. M. Colak, P. Colin, E. Colombo, J. L. Contreras, J. Cortina, S. Covino, P. Cumani, V. D'Elia, P. Da Vela, F. Dazzi, A. De Angelis, B. De Lotto, M. Delfino, J. Delgado, F. Di Pierro, A. Domínguez, D. Dominis Prester, D. Dorner, M. Doro, S. Einecke, D. Elsaesser, V. Fallah Ramazani, A. Fattorini, A. Fernández-Barral, G. Ferrara, D. Fidalgo, L. Foffano, M. V. Fonseca, L. Font, C. Fruck, S. Gallozzi, R. J. García López, M. Garczarczyk, M. Gaug, P. Giammaria, N. Godinović, D. Guberman, D. Hadasch, A. Hahn, T. Hassan, M. Hayashida, J. Herrera, J. Hoang, D. Hrupec, S. Inoue, K. Ishio, Y. Iwamura, Y. Konno, H. Kubo, J. Kushida, A. Lamastra, D. Lelas, F. Leone, E. Lindfors, S. Lombardi, F. Longo, M. López, C. Maggio, P. Majumdar, M. Makariev, G. Maneva, M. Manganaro, K. Mannheim, L. Maraschi, M. Mariotti, M. Martínez, S. Masuda, D. Mazin, K. Mielke, M. Minev, J. M. Miranda, R. Mirzoyan, A. Moralejo, V. Moreno, E. Moretti, V. Neustroev, A. Niedzwiecki, M. Nievas Rosillo, C. Nigro, K. Nilsson, D. Ninci, K. Nishijima, K. Noda, L. Nogués, S. Paiano, J. Palacio, D. Paneque, R. Paoletti, J. M. Paredes, G. Pedalletti, P. Peñil, M. Peresano, M. Persic, K. Pfrang, P. G.

- Prada Moroni, E. Prandini, I. Puljak, J. R. Garcia, W. Rhode, M. Ribó, J. Rico, C. Righi, A. Rugliancich, L. Saha, T. Saito, K. Satalecka, T. Schweizer, J. Sitarek, I. Šnidarić, D. Sobczynska, A. Stamerra, M. Strzys, T. Surić, F. Tavecchio, P. Temnikov, T. Terzić, M. Teshima, N. Torres-Albá, S. Tsujimoto, G. Vanzo, M. Vazquez Acosta, I. Vovk, J. E. Ward, M. Will, D. Zarić, and M. Cerruti.
The Blazar TXS 0506+056 Associated with a High-energy Neutrino: Insights into Extragalactic Jets and Cosmic-Ray Acceleration.
ApJL, 863:L10, August 2018.
- [18] A. T. Araudo, V. Bosch-Ramon, and G. E. Romero.
Gamma rays from cloud penetration at the base of AGN jets.
A&A, 522:A97, November 2010.
- [19] A. T. Araudo, V. Bosch-Ramon, and G. E. Romero.
Gamma-ray emission from massive stars interacting with active galactic nuclei jets.
MNRAS, 436:3626–3639, December 2013.
- [20] K. A. Arnaud.
XSPEC: The First Ten Years.
In G. H. Jacoby and J. Barnes, editors, *Astronomical Data Analysis Software and Systems V*, volume 101 of *Astronomical Society of the Pacific Conference Series*, page 17, 1996.
- [21] W. B. Atwood, A. A. Abdo, M. Ackermann, W. Althouse, B. Anderson, M. Axelsson, L. Baldini, J. Ballet, D. L. Band, G. Barbiellini, and et al.
The Large Area Telescope on the Fermi Gamma-Ray Space Telescope Mission.
ApJ, 697:1071–1102, June 2009.
- [22] W. B. Atwood, A. A. Abdo, M. Ackermann, W. Althouse, B. Anderson, M. Axelsson, L. Baldini, J. Ballet, D. L. Band, G. Barbiellini, and et al.
The Large Area Telescope on the Fermi Gamma-Ray Space Telescope Mission.
ApJ, 697:1071–1102, June 2009.
- [23] Matthew G. Baring, Markus Böttcher, and Errol J. Summerlin.
Probing acceleration and turbulence at relativistic shocks in blazar jets.
MNRAS, 464(4):4875–4894, Feb 2017.

- [24] M. V. Barkov, F. A. Aharonian, and V. Bosch-Ramon.
Gamma-ray Flares from Red Giant/Jet Interactions in Active Galactic Nuclei.
ApJ, 724:1517–1523, December 2010.
- [25] J. H. Beall.
A Review of Astrophysical Jets.
In *Proceedings of the XII Multifrequency Behaviour of High Energy Cosmic Sources Workshop. 12-17 June*, page 62, Jun 2017.
- [26] J. H. Beall and W. Bednarek.
On the Hadronic Beam Model for Gamma-Ray Production in Blazars.
ApJ, 510:188–196, January 1999.
- [27] W. Bednarek and P. Banasiński.
Non-thermal Radiation from Collisions of Compact Objects with Intermediate-scale Jets in Active Galaxies.
ApJ, 807:168, July 2015.
- [28] W. Bednarek and R. J. Protheroe.
Gamma-rays from interactions of stars with active galactic nucleus jets.
MNRAS, 287:L9–L13, May 1997.
- [29] J. Bednarz and M. Ostrowski.
Energy Spectra of Cosmic Rays Accelerated at Ultrarelativistic Shock Waves.
Phys. Rev. Lett., 80(18):3911–3914, May 1998.
- [30] A. R. Bell.
The acceleration of cosmic rays in shock fronts - I.
MNRAS, 182:147–156, Jan 1978.
- [31] W. Bhattacharyya and N. Gupta.
Proton Synchrotron Radiation from Extended Jets of PKS 0637-752 and 3C 273.
ApJ, 817:121, February 2016.
- [32] Roger Blandford and David Eichler.
Particle acceleration at astrophysical shocks: A theory of cosmic ray origin.
Phys. Rep., 154(1):1–75, Oct 1987.

- [33] M. Błażejowski, M. Sikora, R. Moderski, and G. M. Madejski.
Comptonization of Infrared Radiation from Hot Dust by Relativistic
Jets in Quasars.
ApJ, 545:107–116, December 2000.
- [34] M. Błażejowski, M. Sikora, R. Moderski, and G. M. Madejski.
Comptonization of Infrared Radiation from Hot Dust by Relativistic
Jets in Quasars.
ApJ, 545:107–116, December 2000.
- [35] S. D. Bloom and A. P. Marscher.
An Analysis of the Synchrotron Self-Compton Model for the Multi-
Wave Band Spectra of Blazars.
ApJ, 461:657, April 1996.
- [36] M. Bonato, E. Liuzzo, D. Herranz, J. González-Nuevo, L. Bonavera,
M. Tucci, M. Massardi, G. De Zotti, M. Negrello, and M. A. Zwaan.
ALMA photometry of extragalactic radio sources.
MNRAS, 485(1):1188–1195, May 2019.
- [37] M. Böttcher, A. Reimer, K. Sweeney, and A. Prakash.
Leptonic and Hadronic Modeling of Fermi-detected Blazars.
ApJ, 768:54, May 2013.
- [38] A. A. Breeveld, W. Landsman, S. T. Holland, P. Roming, N. P. M. Kuin,
and M. J. Page.
An Updated Ultraviolet Calibration for the Swift/UVOT.
In J. E. McEnery, J. L. Racusin, and N. Gehrels, editors, *American Insti-
tute of Physics Conference Series*, volume 1358 of *American Institute of
Physics Conference Series*, pages 373–376, August 2011.
- [39] Peter Breiding, Markos Georganopoulos, and Eileen T. Meyer.
Blazar Sheath Illumination of the Outer Molecular Torus: A Resolution
of the Seed Photon Problem for the Far-GeV Blazar Flares.
ApJ, 853(1):19, Jan 2018.
- [40] Peter Breiding, Eileen T. Meyer, Markos Georganopoulos, M. E.
Keenan, N. S. DeNigris, and Jennifer Hewitt.
Fermi Non-detections of Four X-Ray Jet Sources and Implications for
the IC/CMB Mechanism.

- ApJ*, 849(2):95, Nov 2017.
- [41] A. M. Brown.
Locating the γ -ray emission region of the flat spectrum radio quasar PKS 1510-089.
MNRAS, 431:824–835, May 2013.
- [42] W. Cash.
Parameter estimation in astronomy through application of the likelihood ratio.
ApJ, 228:939–947, March 1979.
- [43] A. Celotti and G. Ghisellini.
The power of blazar jets.
MNRAS, 385:283–300, March 2008.
- [44] A. Celotti and G. Ghisellini.
The power of blazar jets.
MNRAS, 385:283–300, March 2008.
- [45] Annalisa Celotti, Gabriele Ghisellini, and Marco Chiaberge.
Large-scale jets in active galactic nuclei: multiwavelength mapping.
MNRAS, 321(1):L1–L5, Feb 2001.
- [46] M. Cerruti, A. Zech, C. Boisson, G. Emery, S. Inoue, and J.-P. Lenain.
Lepto-hadronic single-zone models for the electromagnetic and neutrino emission of TXS 0506+056.
ArXiv e-prints, July 2018.
- [47] M. Cerruti, A. Zech, C. Boisson, G. Emery, S. Inoue, and J.-P. Lenain.
Leptohadronic single-zone models for the electromagnetic and neutrino emission of TXS 0506+056.
MNRAS, 483:L12–L16, February 2019.
- [48] Marco Chiaberge and Gabriele Ghisellini.
Rapid variability in the synchrotron self-Compton model for blazars.
MNRAS, 306(3):551–560, Jul 1999.
- [49] L. Costamante, S. Cutini, G. Tosti, E. Antolini, and A. Tramacere.
On the origin of gamma-rays in Fermi blazars: beyond the broad-line region.

- MNRAS*, 477(4):4749–4767, Jul 2018.
- [50] A. Dar and A. Laor.
Hadronic Production of TeV Gamma-Ray Flares from Blazars.
ApJL, 478:L5–L8, March 1997.
- [51] Elisabete M. de Gouveia Dal Pino.
Astrophysical jets and outflows.
Advances in Space Research, 35(5):908–924, Jan 2005.
- [52] V. M. de la Cita, V. Bosch-Ramon, X. Paredes-Fortuny, D. Khangulyan,
and M. Perucho.
Coupling hydrodynamics and radiation calculations for star-jet inter-
actions in active galactic nuclei.
A&A, 591:A15, June 2016.
- [53] N. Ding, Q. S. Gu, X. F. Geng, Ding-Rong Xiong, R. Xue, X. Y. Wang,
and X. T. Guo.
Exploring the Origin of Multiwavelength Activities of High-redshift
Flat-spectrum Radio Quasar PKS 1502+106 during 20142018.
ApJ, 881(2):125, Aug 2019.
- [54] A. Domínguez, J. R. Primack, D. J. Rosario, F. Prada, R. C. Gilmore,
S. M. Faber, D. C. Koo, R. S. Somerville, M. A. Pérez-Torres, P. Pérez-
González, J.-S. Huang, M. Davis, P. Guhathakurta, P. Barmby, C. J.
Conselice, M. Lozano, J. A. Newman, and M. C. Cooper.
Extragalactic background light inferred from AEGIS galaxy-SED-type
fractions.
MNRAS, 410:2556–2578, February 2011.
- [55] Alina-C. Donea and R. J. Protheroe.
Radiation fields of disk, BLR and torus in quasars and blazars: impli-
cations for γ -ray absorption.
Astroparticle Physics, 18(4):377–393, Jan 2003.
- [56] M. J. Drinkwater, R. L. Webster, P. J. Francis, J. J. Condon, S. L. Ellison,
D. L. Jauncey, J. Lovell, B. A. Peterson, and A. Savage.
The Parkes Half-Jansky Flat-Spectrum Sample.
MNRAS, 284:85–125, January 1997.

- [57] L. Oc. Drury.
REVIEW ARTICLE: An introduction to the theory of diffusive shock acceleration of energetic particles in tenuous plasmas.
Reports on Progress in Physics, 46(8):973–1027, Aug 1983.
- [58] Donald C. Ellison and Glen P. Double.
Diffusive shock acceleration in unmodified relativistic, oblique shocks.
Astroparticle Physics, 22(3-4):323–338, Nov 2004.
- [59] Donald C. Ellison, Frank C. Jones, and Stephen P. Reynolds.
First-Order Fermi Particle Acceleration by Relativistic Shocks.
ApJ, 360:702, Sep 1990.
- [60] Justin D. Finke.
External Compton Scattering in Blazar Jets and the Location of the Gamma-Ray Emitting Region.
ApJ, 830(2):94, Oct 2016.
- [61] E. L. Fitzpatrick.
Correcting for the Effects of Interstellar Extinction.
PASP, 111:63–75, January 1999.
- [62] L. Foschini, G. Bonnoli, G. Ghisellini, G. Tagliaferri, F. Tavecchio, and A. Stamerra.
Fermi/LAT detection of extraordinary variability in the gamma-ray emission of the blazar PKS 1510-089.
A&A, 555:A138, July 2013.
- [63] L. Foschini, G. Ghisellini, F. Tavecchio, G. Bonnoli, and A. Stamerra.
Search for the shortest variability at gamma rays in flat-spectrum radio quasars.
A&A, 530:A77, June 2011.
- [64] S. Gao, A. Fedynitch, W. Winter, and M. Pohl.
Interpretation of the coincident observation of a high energy neutrino and a bright flare.
ArXiv e-prints, July 2018.
- [65] S. Gao, A. Fedynitch, W. Winter, and M. Pohl.
Modelling the coincident observation of a high-energy neutrino and a bright blazar flare.

- Nature Astronomy*, 3:88–92, January 2019.
- [66] S. Gasparyan, N. Sahakyan, V. Baghmanyanyan, and D. Zargaryan.
On the Multiwavelength Emission from CTA 102.
ApJ, 863:114, August 2018.
- [67] N. Gehrels, G. Chincarini, P. Giommi, K. O. Mason, J. A. Nousek, A. A. Wells, N. E. White, S. D. Barthelmy, D. N. Burrows, L. R. Cominsky, K. C. Hurley, F. E. Marshall, P. Mészáros, P. W. A. Roming, L. Angelini, L. M. Barbier, T. Belloni, S. Campana, P. A. Caraveo, M. M. Chester, O. Citterio, T. L. Cline, M. S. Cropper, J. R. Cummings, A. J. Dean, E. D. Feigelson, E. E. Fenimore, D. A. Frail, A. S. Fruchter, G. P. Garmire, K. Gendreau, G. Ghisellini, J. Greiner, J. E. Hill, S. D. Hunsberger, H. A. Krimm, S. R. Kulkarni, P. Kumar, F. Lebrun, N. M. Lloyd-Ronning, C. B. Markwardt, B. J. Mattson, R. F. Mushotzky, J. P. Norris, J. Osborne, B. Paczynski, D. M. Palmer, H.-S. Park, A. M. Parsons, J. Paul, M. J. Rees, C. S. Reynolds, J. E. Rhoads, T. P. Sasseen, B. E. Schaefer, A. T. Short, A. P. Smale, I. A. Smith, L. Stella, G. Tagliaferri, T. Takahashi, M. Tashiro, L. K. Townsley, J. Tueller, M. J. L. Turner, M. Vietri, W. Voges, M. J. Ward, R. Willingale, F. M. Zerbi, and W. W. Zhang.
The Swift Gamma-Ray Burst Mission.
ApJ, 611:1005–1020, August 2004.
- [68] G. Ghisellini, L. Maraschi, and A. Treves.
Inhomogeneous synchrotron-self-Compton models and the problem of relativistic beaming of BL Lac objects.
A&A, 146:204–212, May 1985.
- [69] G. Ghisellini and F. Tavecchio.
Canonical high-power blazars.
MNRAS, 397:985–1002, August 2009.
- [70] G. Ghisellini and F. Tavecchio.
Canonical high-power blazars.
MNRAS, 397(2):985–1002, Aug 2009.
- [71] G. Ghisellini and F. Tavecchio.
Fermi/LAT broad emission line blazars.
MNRAS, 448:1060–1077, April 2015.

-
- [72] Gabriele Ghisellini.
Radiative Processes in High Energy Astrophysics, volume 873.
2013.
- [73] F. Halzen and D. Hooper.
High energy neutrinos from the TeV Blazar 1ES 159 + 650.
Astroparticle Physics, 23:537–542, July 2005.
- [74] F. Halzen and A. Kheirandish.
High-energy Neutrinos from Recent Blazar Flares.
ApJ, 831:12, November 2016.
- [75] M. J. Hardcastle, M. Birkinshaw, R. A. Cameron, D. E. Harris, L. W. Looney, and D. M. Worrall.
Magnetic Field Strengths in the Hot Spots and Lobes of Three Powerful Fanaroff-Riley Type II Radio Sources.
ApJ, 581:948–973, December 2002.
- [76] D. E. Harris and H. Krawczynski.
X-Ray Emission Processes in Radio Jets.
ApJ, 565(1):244–255, Jan 2002.
- [77] D. E. Harris and Henric Krawczynski.
X-Ray Emission from Extragalactic Jets.
ARAA, 44(1):463–506, Sep 2006.
- [78] J. Harris, M. K. Daniel, and P. M. Chadwick.
Identifying Breaks and Curvature in the Fermi Spectra of Bright Flat Spectrum Radio Quasars.
ApJ, 761(1):2, Dec 2012.
- [79] M. Hayashida, K. Nalewajko, and et al.
Rapid Variability of Blazar 3C 279 during Flaring States in 2013-2014 with Joint Fermi-LAT, NuSTAR, Swift, and Ground-Based Multi-wavelength Observations.
ApJ, 807:79, July 2015.
- [80] H.-N. He, Y. Inoue, S. Inoue, and Y.-F. Liang.
High-energy neutrino flare from cloud-jet interaction in the blazar PKS 0502+049.
ArXiv e-prints, August 2018.

- [81] IceCube Collaboration.
Evidence for High-Energy Extraterrestrial Neutrinos at the IceCube Detector.
Science, 342:1242856, November 2013.
- [82] IceCube Collaboration.
Neutrino emission from the direction of the blazar txs 0506+056 prior to the icecube-170922a alert.
Science, 361(6398):147–151, 2018.
- [83] IceCube Collaboration, MAGIC, FERMI -LAT, MAGIC, AGILE, ASAS-SN, HAWC, H.E.S.S., INTEGRAL, KANATA, KISO, KAPTEYN, LIVERPOOL TELESCOPE, SUBARU, SWIFT/NUSTAR, VERITAS, and VLA/17B-403.
Multimessenger observations of a flaring blazar coincident with high-energy neutrino icecube-170922a.
Science, 361(6398), 2018.
- [84] S. Inoue and F. Takahara.
Electron Acceleration and Gamma-Ray Emission from Blazars.
ApJ, 463:555, June 1996.
- [85] S. Inoue and F. Takahara.
Electron Acceleration and Gamma-Ray Emission from Blazars.
ApJ, 463:555, June 1996.
- [86] Frank C. Jones and Donald C. Ellison.
The plasma physics of shock acceleration.
Space Science Reviews, 58(1):259–346, Dec 1991.
- [87] M. Kadler, F. Krauß, K. Mannheim, R. Ojha, C. Müller, R. Schulz, G. Anton, W. Baumgartner, T. Beuchert, S. Buson, B. Carpenter, T. Eberl, P. G. Edwards, D. Eisenacher Glawion, D. Elsässer, N. Gehrels, C. Gräfe, S. Gulyaev, H. Hase, S. Horiuchi, C. W. James, A. Kappes, A. Kappes, U. Katz, A. Kreikenbohm, M. Kreter, I. Kreykenbohm, M. Langejahn, K. Leiter, E. Litzinger, F. Longo, J. E. J. Lovell, J. McEnery, T. Natusch, C. Phillips, C. Plötz, J. Quick, E. Ros, F. W. Stecker, T. Steinbring, J. Stevens, D. J. Thompson, J. Trüstedt, A. K. Tzioumis, S. Weston, J. Wilms, and J. A. Zensus.

-
- Coincidence of a high-fluence blazar outburst with a PeV-energy neutrino event.
Nature Physics, 12:807–814, August 2016.
- [88] A. Kappes, J. Hinton, C. Stegmann, and F. A. Aharonian.
Potential Neutrino Signals from Galactic γ -Ray Sources.
ApJ, 656:870–878, February 2007.
- [89] Jun Kataoka and Łukasz Stawarz.
X-Ray Emission Properties of Large-Scale Jets, Hot Spots, and Lobes in Active Galactic Nuclei.
ApJ, 622(2):797–810, Apr 2005.
- [90] Navpreet Kaur and Kiran S. Baliyan.
CTA 102 in exceptionally high state during 2016-2017.
A&A, 617:A59, Sep 2018.
- [91] A. Keivani, K. Murase, M. Petropoulou, D. B. Fox, S. B. Cenko, S. Chaty, A. Coleiro, J. J. DeLaunay, S. Dimitrakoudis, P. A. Evans, J. A. Kennea, F. E. Marshall, A. Mastichiadis, J. P. Osborne, M. Santander, A. Tohuvavohu, and C. F. Turley.
A Multimessenger Picture of the Flaring Blazar TXS 0506+056: Implications for High-energy Neutrino Emission and Cosmic-Ray Acceleration.
ApJ, 864:84, September 2018.
- [92] S. R. Kelner, F. A. Aharonian, and V. V. Bugayov.
Energy spectra of gamma rays, electrons, and neutrinos produced at proton-proton interactions in the very high energy regime.
Phys. Rev. D, 74(3):034018, August 2006.
- [93] B. Khiali and E. M. de Gouveia Dal Pino.
High-energy neutrino emission from the core of low luminosity AGNs triggered by magnetic reconnection acceleration.
MNRAS, 455:838–845, January 2016.
- [94] J. G. Kirk, A. W. Guthmann, Y. A. Gallant, and A. Achterberg.
Particle Acceleration at Ultrarelativistic Shocks: An Eigenfunction Method.
ApJ, 542(1):235–242, Oct 2000.
-

- [95] J. G. Kirk and A. F. Heavens.
Particle acceleration at oblique shock fronts.
MNRAS, 239:995–1011, Aug 1989.
- [96] Susanna Kohler and Krzysztof Nalewajko.
Turbulent spectra of the brightest gamma-ray flares of blazars.
MNRAS, 449(3):2901–2909, May 2015.
- [97] Masaaki Kusunose and Fumio Takahara.
A Photohadronic Model of the Large-scale Jet of PKS 0637-752.
ApJ, 835(1):20, Jan 2017.
- [98] Xiaofeng Li, P. Mohan, T. An, Xiaoyu Hong, Xiaopeng Cheng, Jun Yang, Yingkang Zhang, Zhongli Zhang, and Wei Zhao.
Imaging and Variability Studies of CTA 102 during the 2016 January γ -ray Flare.
ApJ, 854(1):17, Feb 2018.
- [99] Y.-F. Liang, H.-N. He, N.-H. Liao, Y.-L. Xin, Q. Yuan, and Y.-Z. Fan.
Search for GeV flare coincident with the IceCube neutrino flare.
ArXiv e-prints, July 2018.
- [100] N.-H. Liao, Y.-L. Xin, Y.-F. Liang, X.-L. Guo, S. Li, H.-N. He, Q. Yuan, and Y.-Z. Fan.
Active galactic nuclei with GeV activities and the PeV neutrino source candidate TXS 0506+056.
ArXiv e-prints, July 2018.
- [101] B. Lott, L. Escande, S. Larsson, and J. Ballet.
An adaptive-binning method for generating constant-uncertainty/constant-significance light curves with Fermi-LAT data.
A&A, 544:A6, August 2012.
- [102] K. Mannheim.
The proton blazar.
A&A, 269:67–76, March 1993.
- [103] K. Mannheim.
High-energy neutrinos from extragalactic jets.
Astroparticle Physics, 3:295–302, May 1995.

-
- [104] K. Mannheim and P. L. Biermann.
Photomeson production in active galactic nuclei.
A&A, 221:211–220, September 1989.
- [105] L. Maraschi, G. Ghisellini, and A. Celotti.
A jet model for the gamma-ray emitting blazar 3C 279.
ApJL, 397:L5–L9, September 1992.
- [106] E. Massaro, M. Perri, P. Giommi, R. Nesci, and F. Verrecchia.
Log-parabolic spectra and particle acceleration in blazars. II. The Bep-
poSAX wide band X-ray spectra of Mkn 501.
A&A, 422:103–111, July 2004.
- [107] Eileen T. Meyer, Peter Breiding, Markos Georganopoulos, Iván Oteo,
Martin A. Zwaan, Robert Laing, Leith Godfrey, and R. J. Ivison.
New ALMA and Fermi/LAT Observations of the Large-scale Jet of PKS
0637-752 Strengthen the Case Against the IC/CMB Model.
ApJL, 835(2):L35, Feb 2017.
- [108] Eileen T. Meyer and Markos Georganopoulos.
Fermi Rules Out the Inverse Compton/CMB Model for the Large-scale
Jet X-Ray Emission of 3C 273.
ApJL, 780(2):L27, Jan 2014.
- [109] Eileen T. Meyer, Markos Georganopoulos, William B. Sparks, Leith
Godfrey, James E. J. Lovell, and Eric Perlman.
Ruling out IC/CMB X-rays in PKS 0637-752 and the Implications for
TeV Emission from Large-scale Quasar Jets.
ApJ, 805(2):154, Jun 2015.
- [110] Manuel Meyer, Jeffrey D. Scargle, and Roger D. Blandford.
Characterizing the Gamma-Ray Variability of the Brightest Flat Spec-
trum Radio Quasars Observed with the Fermi LAT.
ApJ, 877(1):39, May 2019.
- [111] A. Mücke and R. J. Protheroe.
A proton synchrotron blazar model for flaring in Markarian 501.
Astroparticle Physics, 15:121–136, March 2001.
- [112] A. Mücke, R. J. Protheroe, R. Engel, J. P. Rachen, and T. Stanev.

- BL Lac objects in the synchrotron proton blazar model.
Astroparticle Physics, 18:593–613, March 2003.
- [113] K. Murase, D. Guetta, and M. Ahlers.
Hidden Cosmic-Ray Accelerators as an Origin of TeV-PeV Cosmic Neutrinos.
Physical Review Letters, 116(7):071101, February 2016.
- [114] K. Murase, F. Oikonomou, and M. Petropoulou.
Blazar Flares as an Origin of High-energy Cosmic Neutrinos?
ApJ, 865:124, October 2018.
- [115] K. Nalewajko.
The brightest gamma-ray flares of blazars.
MNRAS, 430:1324–1333, April 2013.
- [116] M. Nenkova, M. M. Sirocky, R. Nikutta, Ž. Ivezić, and M. Elitzur.
AGN Dusty Tori. II. Observational Implications of Clumpiness.
ApJ, 685:160–180, September 2008.
- [117] A. Y. K. N. Oshlack, R. L. Webster, and M. T. Whiting.
Black Hole Mass Estimates of Radio-selected Quasars.
ApJ, 576:81–88, September 2002.
- [118] L. Pacciani, F. Tavecchio, I. Donnarumma, A. Stamerra, L. Carrasco, E. Recillas, A. Porras, and M. Uemura.
Exploring the Blazar Zone in High-energy Flares of FSRQs.
ApJ, 790:45, August 2014.
- [119] P. Padovani, P. Giommi, E. Resconi, T. Glauch, B. Arsioli, N. Sahakyan, and M. Huber.
Dissecting the region around IceCube-170922A: the blazar TXS 0506+056 as the first cosmic neutrino source.
ArXiv e-prints, July 2018.
- [120] P. Padovani, E. Resconi, P. Giommi, B. Arsioli, and Y. L. Chang.
Extreme blazars as counterparts of icecube astrophysical neutrinos.
Monthly Notices of the Royal Astronomical Society, 457(4):3582–3592, 2016.
- [121] Paolo Padovani and Paolo Giommi.

- The Connection between X-Ray- and Radio-selected BL Lacertae Objects.
ApJ, 444:567, May 1995.
- [122] S. Paiano, R. Falomo, A. Treves, and R. Scarpa.
The Redshift of the BL Lac Object TXS 0506+056.
ApJL, 854:L32, February 2018.
- [123] Vaidehi S. Paliya.
Fermi-Large Area Telescope Observations of the Exceptional Gamma-Ray Flare from 3C 279 in 2015 June.
ApJL, 808(2):L48, Aug 2015.
- [124] Vaidehi S. Paliya, S. Sahayanathan, and C. S. Stalin.
Multi-Wavelength Observations of 3C 279 During the Extremely Bright Gamma-Ray Flare in 2014 March-April.
ApJ, 803(1):15, Apr 2015.
- [125] E. Pian, R. Falomo, and A. Treves.
Hubble Space Telescope ultraviolet spectroscopy of blazars: emission-line properties and black hole masses.
MNRAS, 361:919–926, August 2005.
- [126] Raj Prince, Gayathri Raman, Joachim Hahn, Nayantara Gupta, and Pratik Majumdar.
Fermi-Large Area Telescope Observations of the Brightest Gamma-Ray Flare Ever Detected from CTA 102.
ApJ, 866(1):16, Oct 2018.
- [127] B. Rani, B. Lott, T. P. Krichbaum, L. Fuhrmann, and J. A. Zensus.
Constraining the location of rapid gamma-ray flares in the flat spectrum radio quasar 3C 273.
A&A, 557:A71, September 2013.
- [128] B. Rani, B. Lott, T. P. Krichbaum, L. Fuhrmann, and J. A. Zensus.
Constraining the location of rapid gamma-ray flares in the flat spectrum radio quasar 3C 273.
A&A, 557:A71, Sep 2013.
- [129] A. Reimer.

- The Redshift Dependence of Gamma-Ray Absorption in the Environments of Strong-Line AGNs.
ApJ, 665(2):1023–1029, Aug 2007.
- [130] Frank M. Rieger, Valentí Bosch-Ramon, and Peter Duffy.
Fermi acceleration in astrophysical jets.
Ap&SS, 309(1-4):119–125, Jun 2007.
- [131] N. Sahakyan.
Lepto-hadronic γ -Ray and Neutrino Emission from the Jet of TXS 0506+056.
ApJ, 866:109, October 2018.
- [132] N. Sahakyan.
Origin of the multiwavelength emission of PKS 0502+049.
A&A, 622:A144, Feb 2019.
- [133] N. Sahakyan and S. Gasparyan.
High energy gamma-ray emission from PKS 1441+25.
MNRAS, 470:2861–2869, September 2017.
- [134] N. Sahakyan, G. Piano, and M. Tavani.
Hadronic Gamma-Ray and Neutrino Emission from Cygnus X-3.
ApJ, 780:29, January 2014.
- [135] S. Saito, Ł. Stawarz, and et al.
Very Rapid High-amplitude Gamma-Ray Variability in Luminous Blazar PKS 1510-089 Studied with Fermi-LAT.
ApJL, 766:L11, March 2013.
- [136] E. F. Schlafly and D. P. Finkbeiner.
Measuring Reddening with Sloan Digital Sky Survey Stellar Spectra and Recalibrating SFD.
ApJ, 737:103, August 2011.
- [137] A. Shukla, K. Mannheim, S. R. Patel, J. Roy, V. R. Chitnis, D. Dorner, A. R. Rao, G. C. Anupama, and C. Wendel.
Short-timescale γ -Ray Variability in CTA 102.
ApJL, 854(2):L26, Feb 2018.

- [138] M. Sikora, M. C. Begelman, and M. J. Rees.
Comptonization of diffuse ambient radiation by a relativistic jet: The source of gamma rays from blazars?
ApJ, 421:153–162, January 1994.
- [139] M. Sikora, Ł. Stawarz, R. Moderski, K. Nalewajko, and G. M. Madejski.
Constraining Emission Models of Luminous Blazar Sources.
ApJ, 704:38–50, October 2009.
- [140] Łukasz Stawarz, Marek Sikora, Michał Ostrowski, and Mitchell C. Begelman.
On Multiwavelength Emission of Large-Scale Quasar Jets.
ApJ, 608(1):95–107, Jun 2004.
- [141] Errol J. Summerlin and Matthew G. Baring.
Diffusive Acceleration of Particles at Oblique, Relativistic, Magnetohydrodynamic Shocks.
ApJ, 745(1):63, Jan 2012.
- [142] F. Tavecchio, J. Becerra-Gonzalez, G. Ghisellini, A. Stamerra, G. Bonoli, L. Foschini, and L. Maraschi.
On the origin of the γ -ray emission from the flaring blazar PKS 1222+216.
A&A, 534:A86, Oct 2011.
- [143] F. Tavecchio and G. Ghisellini.
High-energy cosmic neutrinos from spine-sheath BL Lac jets.
MNRAS, 451:1502–1510, August 2015.
- [144] F. Tavecchio, G. Ghisellini, and D. Guetta.
Structured Jets in BL Lac Objects: Efficient PeV Neutrino Factories?
ApJL, 793:L18, September 2014.
- [145] Fabrizio Tavecchio, Laura Maraschi, Rita M. Sambruna, and C. Megan Urry.
The X-Ray Jet of PKS 0637-752: Inverse Compton Radiation from the Cosmic Microwave Background?
ApJL, 544(1):L23–L26, Nov 2000.
- [146] The Fermi-LAT collaboration.

- Fermi Large Area Telescope Fourth Source Catalog.
arXiv e-prints, page arXiv:1902.10045, Feb 2019.
- [147] C. M. Urry and P. Padovani.
Unified Schemes for Radio-Loud Active Galactic Nuclei.
PASP, 107:803, September 1995.
- [148] Daniel E. Vanden Berk, Gordon T. Richards, Amanda Bauer, Michael A. Strauss, Donald P. Schneider, Timothy M. Heckman, Donald G. York, Patrick B. Hall, Xiaohui Fan, G. R. Knapp, Scott F. Anderson, James Annis, Neta A. Bahcall, Mariangela Bernardi, John W. Briggs, J. Brinkmann, Robert Brunner, Scott Burles, Larry Carey, Francisco J. Castander, A. J. Connolly, J. H. Crocker, István Csabai, Mamoru Doi, Douglas Finkbeiner, Scott Friedman, Joshua A. Frieman, Masataka Fukugita, James E. Gunn, G. S. Hennessy, Željko Ivezić, Stephen Kent, Peter Z. Kunszt, D. Q. Lamb, R. French Leger, Daniel C. Long, Jon Loveday, Robert H. Lupton, Avery Meiksin, Aronne Merelli, Jeffrey A. Munn, Heidi Jo Newberg, Matt Newcomb, R. C. Nichol, Russell Owen, Jeffrey R. Pier, Adrian Pope, Constance M. Rockosi, David J. Schlegel, Walter A. Siegmund, Stephen Smee, Yehuda Snir, Chris Stoughton, Christopher Stubbs, Mark SubbaRao, Alexander S. Szalay, Gyula P. Szokoly, Christy Tremonti, Alan Uomoto, Patrick Waddell, Brian Yanny, and Wei Zheng.
Composite Quasar Spectra from the Sloan Digital Sky Survey.
AJ, 122(2):549–564, Aug 2001.
- [149] K. Wang, R.-Y. Liu, Z. Li, X.-Y. Wang, and Z.-G. Dai.
Jet-cloud/star interaction as an interpretation of neutrino outburst from the blazar TXS 0506+056.
ArXiv e-prints, September 2018.
- [150] X.-Y. Wang and R.-Y. Liu.
Tidal disruption jets of supermassive black holes as hidden sources of cosmic rays: Explaining the IceCube TeV-PeV neutrinos.
Phys. Rev. D, 93(8):083005, April 2016.
- [151] V. Zabalza.
naima: a python package for inference of relativistic particle energy distributions from observed nonthermal spectra.

- Proc. of International Cosmic Ray Conference 2015*, page in press, 2015.
- [152] M. Zacharias, M. Böttcher, F. Jankowsky, J. P. Lenain, S. J. Wagner, and A. Wierzcholska.
Cloud Ablation by a Relativistic Jet and the Extended Flare in CTA 102 in 2016 and 2017.
ApJ, 851(2):72, Dec 2017.
- [153] M. Zacharias, M. Böttcher, F. Jankowsky, J. P. Lenain, S. J. Wagner, and A. Wierzcholska.
The Extended Flare in CTA 102 in 2016 and 2017 within a Hadronic Model through Cloud Ablation by the Relativistic Jet.
ApJ, 871(1):19, Jan 2019.
- [154] M. Zamaninasab, E. Clausen-Brown, T. Savolainen, and A. Tchekhovskoy.
Dynamically important magnetic fields near accreting supermassive black holes.
Nature, 510(7503):126–128, Jun 2014.
- [155] D. Zargaryan, S. Gasparyan, V. Baghmanyanyan, and N. Sahakyan.
Comparing 3C 120 jet emission at small and large scales.
A&A, 608:A37, Dec 2017.

